p-wave size resonances observed by the (p, n) reaction for 2.6- to 7-MeV protons incident on isotopes of Sn†

C. H. Johnson, J. K. Bair, C. M. Jones, S. K. Penny, and D. W. Smith*
Oak Ridge National Laboratory, Oak Ridge, Tennessee 37830
(Received 26 July 1976)

The ^{117,118,119,120,122,124}Sn(p, n) cross sections were measured with ~ 100-keV resolution for 2.6- to 7-MeV protons with systematic uncertainties of less than ± 1%. An exact sequence of broad maxima in the strength functions is observed with the energies at the peaks ranging from 5.45 MeV for ^{124}Sn to 6.15 MeV for ^{117}Sn. These are interpreted in terms of the $3p$ quasibound proton state in the optical-model potential. Values of VR^2 for the real well at the resonance energies are determined unambiguously to ± 1% and range from 2120 MeV fm^2 for ^{117}Sn to 2215 MeV fm^2 for ^{124}Sn. For an assumed Woods-Saxon real-well geometry of radius $1.2A^{1/3}$ fm and diffuseness 0.73 fm, the volume integral per nucleon is 513 ± 1 MeV fm^3 at each resonant maximum. The isotopic sequence of resonances appears to be unrelated to the asymmetry potential. The volume integral per nucleon of the surface absorptive potential is 80 ± 4 MeV fm^3 and the diffuseness is 0.4 ± 0.1 fm, where the uncertainties include ambiguities in the other model parameters. Comparisons with scattering at higher energies give evidence for an l dependence in both the real and absorptive potentials. Comparison with the neutron $3p$ size resonance near $A = 100$ is consistent with a 24-MeV asymmetry term in the real potential and a 15-MeV asymmetry term in the absorptive potential. Statistical model analyses of γ-ray and neutron emission from the compound nuclei suggest that the compound temperatures are about a factor of 2 higher than expected. Evidence is found for broad structures at 1 to 1.5 MeV excitation in ^{118,120}Sb. The Appendix includes an evaluation of levels below 2 MeV in ^{117}Sb and ^{119}Sb.

[NUCLEAR REACTIONS $^{117, 118, 119, 120, 122, 124}Sn(p,n)$, E=2.6 to 7 MeV, resolution 70 to 180 keV, enriched targets. Measured total $\sigma_{p,n}$. Deduced energy of $3p$ quasibound proton states in $^{118, 119, 120, 121, 123, 125}$Sb. Statistical model and optical-model analysis, deduced model parameters.]

I. INTRODUCTION

The proton optical-model potential has been very successful for interpreting the average properties of proton interactions with nuclei. It has been used especially for protons incident on nuclei at energies above the Coulomb barrier. Lower energy protons are not sensitive probes of the nucleus because they must penetrate the Coulomb barrier; nevertheless, precision measurements of the total absorption cross sections at sub-Coulomb energies can reveal nuclear properties that may not be detected at higher energies. In particular, single-particle states are expected to be quasibound by the barrier. These may be spread over several MeV by the mixing associated with the absorptive part of the potential but the spreading width should be less than the barrier height for intermediate-weight nuclei, so the resulting resonances, albeit very broad, should be observable.

The problem is to observe the resonances in the presence of the Coulomb barrier. In one sense that is easy because the compound nuclei probably decay by neutron emission and can be detected by straightforward measurements of (p,n) cross sections. But that is a first approximation; actually, γ rays compete significantly with neutrons for at least 1 MeV above the (p,n) threshold. Unfortunately, not enough information is available to make straightforward corrections for γ-ray emission. That topic occupies a lot of this report; the results indicate that the nuclear temperatures for the compound nuclei are about a factor of 2 larger than expected, or that the statistical model of nuclear reactions is deficient in some other respect.

Johnson and Kernell[1] observed the first indications of the $3p$ strength-function resonances in isotopes of Sn and predicted on the basis of the optical model that the Sn isotopes would each exhibit a broad resonance with the energy at the peak decreasing from about 6.6 MeV for ^{117}Sn to 5.2 MeV for ^{124}Sn. Actual resonances were not observed because the proton energies were below 5.3 MeV.

We have repeated those measurements with higher precision and extended them to 7 MeV. A remarkably systematic series of peaks are observed for the Sn isotopes and the conditions for resonances appear to require a constant volume integral per nucleon for the real part of the potential. To our knowledge this is the first clear observation of strength-function or size resonances versus the incident particle energy. (The well-known max-

ima first observed by Barschall[2] in the neutron average total cross sections have a different explanation.[3]) The resonances are specifically for p-wave protons. Comparisons with the p-wave size resonance for neutrons and with scattering for all partial waves at higher proton energies give evidence on the isospin and l dependences of the optical-model potential.

II. SUMMARY OF OBSERVED CROSS SECTIONS

The experiment was simple. Protons of known energy between 2.6 and 7 MeV impinged on a given Sn target and neutrons were counted in 4π geometry with known efficiency. The (p,n) cross sections were deduced using the target areal densities and isotopic compositions from Table I. More experimental details are given below but the final cross sections are listed in Table II. These values range from 9 to 187000 μb. (For comparison the earlier values[1] must be decreased 2% because of a change in the detector calibration.)

Figures 1 and 2 show the ratio of these cross sections to a smooth fit to the ^{124}Sn(p,n) excitation function. Interpolations have been made using the empirical relation $\sigma(E) \sim \exp(B/E)$, where B is arbitrary. The arrows in Fig. 1 indicate the known resonant energies for the ground[4,5] and excited[6] analog states and the curves are drawn consistently with the target thicknesses. (The even isotopes have no analog-state resonances at these energies.[6])

Table III summarizes the uncertainties in cross sections. Uncertainties in energies have been transformed to the cross sections at exact proton energies. Above 4 MeV the systematic and random uncertainties combine in quadrature to give less than $\pm 1\%$, except for ^{118}Sn near its threshold. Below 4 MeV the uncertainties tend to be larger because of the decreasing ratio of yield to background. In Figs. 1 and 2 the uncertainties shown by error bars at low energies are actually systematic. The anomalous increase for ^{122}Sn below 3.5 MeV could arise from systematic errors in subtracting backgrounds in either ^{122}Sn or ^{124}Sn. If the error were in ^{124}Sn, the smooth curve below 3.5 MeV would be raised and the points for all of the other isotopes would be lowered.

III. EXPERIMENTAL METHOD AND UNCERTAINTIES

The major uncertainties are systematic and should not all be included in the weighting factors to be used in the least-squares analysis. Our procedure for assigning the individual uncertainties in Table II was to combine in quadrature uncertainties that apply only to the given target and are either random or energy dependent. The remaining systematic uncertainties are listed in Table III and are either constant for a given target or apply equally to all targets and may be energy dependent.

A. Proton energy and charge

Figure 3 shows the experimental geometry. Protons from the nominal 6-MV electrostatic accelerator were analyzed by a magnet having a known[7] saturation curve. We calibrated using the ^{19}F(p,n) threshold at 4234.3 $\pm$0.8 keV.[8] The $\pm$1-keV random error[7] in proton energy was confirmed by the reproducibility in the steeply rising (p,n) excitation functions. Corrections for the average energy loss in the target have negligible uncertainty.[1] The nonlinearities of the excitation functions made it necessary to convert[1] the observed $\bar{\sigma}$ to $\sigma(\bar{E})$; curve f in Fig. 4 shows this correction for ^{124}Sn. The proton charge was measured with an accurate current integrator.

B. Neutron detection

Neutrons were counted in 4π geometry by Macklin's[9] 1.5-m graphite sphere. The detector response is constant to better than 1% from a few keV to 1 MeV but decreases about 7% from 1 to 5 MeV because of neutron leakage from the surface. We determined the absolute efficiency to $\pm$0.6% at an average energy of 500 keV, which is in the flat part of the response curve, using the National Bureau of Standards NBS-II RaBe photoneutron source. DeVolpi and Porges[10] quote absolute yields from NBS-II to $\pm$0.37% from the Argonne National Laboratory and $\pm$0.5% from the National Physical Laboratory of the United Kingdom. We weighted these two values and corrected for the 1620-yr half-life. The counts from this source were corrected for γ rays (0.9%), deadtime (0.22%), room background (0.005%), and absorption of neutrons in the radium of the source (0.04%). At the same

TABLE I. The Sn targets.

A	Enrichment (%)	Areal density (mg/cm^2)	$-Q_{p,n}$ (keV)
117	78.81	3.578 $\pm$0.1%	2525[a]
118	96.61	2.579 $\pm$0.2%	4439[b]
119	83.98	3.197 $\pm$0.2%	1369[a]
120	98.39	3.537 $\pm$0.2%	3463[c]
122	92.25	2.448 $\pm$0.3%	2393[c]
124	94.47	3.634 $\pm$0.2%	1398[c]

[a] Reference 5.

[b] C. H. Johnson, J. K. Bair, and C. M. Jones (unpublished).

[c] N. B. Gove and A. H. Wapstra, Nucl. Data A11, 127 (1972).

TABLE II. The Sn(p,n) cross sections.

^{117}Sn(p,n)		^{118}Sn(p,n)		^{119}Sn(p,n)		^{120}Sn(p,n)		^{122}Sn(p,n)		^{124}Sn(p,n)	
E (keV)	$\sigma,\Delta\sigma$ (mb, ±%)	E (keV)	$\sigma,\Delta\sigma$ (mb, ±%)	E (keV)	$\sigma,\Delta\sigma$ (mb, ±%)	E (keV)	$\sigma,\Delta\sigma$ (mb, ±%)	E (keV)	$\sigma,\Delta\sigma$ (mb, ±%)	E (keV)	$\sigma,\Delta\sigma$ (mb, ±%)
2829	0.014, 16			2619	0.009, 11			2638	0.013, 14	2609	0.013, 10
2944	0.027, 11			2842	0.030, 6			2860	0.43, 7	2948	0.070, 4
3062	0.051, 5.7			3073	0.086, 2.6			2974	0.071, 5	3064	0.115, 2.5
3181	0.089, 4.2			3192	0.141, 1.9			3090	0.120, 2.7	3183	0.187, 1.9
3302	0.155, 3.2			3313	0.226, 1.6			3209	0.195, 1.8	3304	0.294, 1.6
3425	0.258, 2.2			3436	0.347, 1.2			3329	0.297, 1.6	3427	0.451, 1.2
3550	0.412, 1.8			3561	0.532, 1.0	3681	0.596, 0.67	3451	0.459, 1.2	3552	0.689, 1.0
3677	0.636, 1.4			3688	0.803, 0.77	3811	1.043, 0.43	3576	0.683, 0.93	3679	1.029, 0.80
3806	0.950, 1.0			3817	1.184, 0.60	3942	1.602, 0.36	3703	1.019, 0.75	3808	1.499, 0.62
3938	1.388, 0.8			3948	1.705, 0.48	4075	2.358, 0.30	3831	1.449, 0.59	3939	2.148, 0.52
4071	2.039, 0.6			4081	2.449, 0.42	4210	3.380, 0.27	3961	2.094, 0.50	4072	3.046, 0.41
4206	2.923, 0.5	4531	1.38, 2.1	4216	3.447, 0.36	4347	4.761, 0.25	4094	2.947, 0.40	4207	4.272, 0.36
4343	4.144, 0.48	4573	2.50, 0.8	4353	4.799, 0.37	4486	6.528, 0.23	4229	4.154, 0.35	4344	5.830, 0.42
4482	7.045, 0.43	4644	4.08, 0.5	4492	6.660, 0.35	4627	8.817, 0.21	4365	5.686, 0.31	4483	7.820, 0.35
4623	7.743, 0.45	4787	7.59, 0.36	4633	11.50, 0.29	4770	11.92, 0.21	4504	7.656, 0.30	4624	10.45, 0.33
4767	10.29, 0.42	4931	11.54, 0.29	4776	11.78, 0.30	4916	15.63, 0.19	4645	10.18, 0.29	4767	13.60, 0.31
4911	13.68, 0.37	5078	15.73, 0.26	4921	15.35, 0.28	5062	20.33, 0.18	4787	13.33, 0.26	4912	17.69, 0.29
5059	17.90, 0.33	5227	21.00, 0.22	5068	19.95, 0.27	5212	25.90, 0.18	4932	17.32, 0.24	5059	22.66, 0.27
5178	21.84, 0.30	5317	24.61, 0.20	5187	24.24, 0.26	5302	29.73, 0.22	5078	22.22, 0.22	5178	27.25, 0.24
5298	26.67, 0.29	5438	30.26, 0.22	5307	29.24, 0.23	5362	32.40, 0.24	5227	27.95, 0.23	5298	32.63, 0.23
5418	32.01, 0.29	5561	36.61, 0.22	5428	35.20, 0.25	5423	35.30, 0.17	5317	31.96, 0.19	5420	38.60, 0.23
5540	38.25, 0.27	5684	44.35, 0.21	5551	41.60, 0.25	5546	41.72, 0.18	5440	38.05, 0.21	5543	45.43, 0.24
5664	46.31, 0.26	5809	52.82, 0.21	5674	49.11, 0.25	5670	49.13, 0.18	5562	44.78, 0.20	5666	53.26, 0.24
5789	53.79, 0.26	5936	62.29, 0.20	5799	58.49, 0.26	5795	57.08, 0.18	5684	52.46, 0.23	5791	61.32, 0.22
5916	62.31, 0.25	6063	72.05, 0.20	5925	66.31, 0.27	5922	66.16, 0.23	5809	60.73, 0.23	5918	70.89, 0.21
6043	72.25, 0.23	6191	82.79, 0.19	6053	76.15, 0.30	5953	68.39, 0.22	5935	70.36, 0.21	6045	80.82, 0.20
6172	84.29, 0.23	6321	94.05, 0.18	6182	87.13, 0.30	6049	76.03, 0.15	6062	79.84, 0.21	6174	91.65, 0.20
6302	94.01, 0.23	6452	105.9, 0.19	6312	98.79, 0.30	6178	86.95, 0.15	6191	90.70, 0.21	6304	102.7, 0.20
6433	106.7, 0.23	6584	118.2, 0.23	6442	112.0, 0.43	6308	98.67, 0.16	6320	103.1, 0.20	6435	115.1, 0.20
6565	119.9, 0.24	6617	122.0, 0.24	6573	123.5, 0.40	6439	110.7, 0.16	6451	114.7, 0.21	6567	128.3, 0.21
6699	132.7, 0.25	6718	132.1, 0.21	6674	134.1, 0.51	6571	124.0, 0.16	6583	127.7, 0.22	6700	141.8, 0.22
6901	157.6, 0.25	6785	139.6, 0.22	6807	148.3, 0.55	6705	137.8, 0.20	6716	141.9, 0.20	6835	155.7, 0.21
7071	173.6, 0.25	6920	154.6, 0.20	6943	164.4, 0.30	6839	152.1, 0.25	6851	156.4, 0.20	6971	170.8, 0.25
				7079	186.4, 0.23	6975	167.7, 0.22	6986	171.6, 0.27	7107	187.1, 0.31

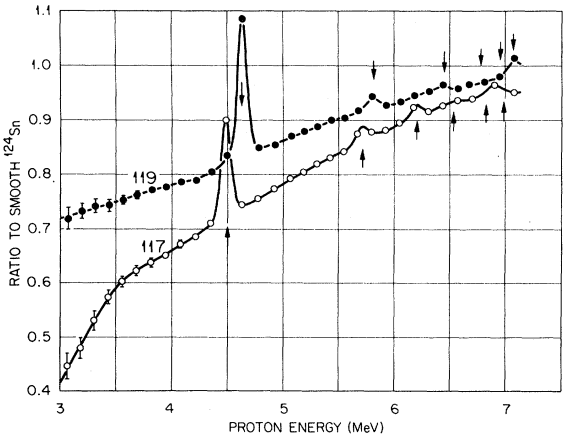

FIG. 1. Odd Sn targets, ratios of the (p,n) cross sections to a smooth curve for ^{124}Sn(p,n). Interpolation was done by the empirical relation $\sigma \sim \exp(B/E)$. Arrows indicate energies of known isobaric analog resonances.

time we established our own RaBe photoneutron and PuBe substandards for later recalibrations. (PuBe sources grow in strength[11]; comparisons with the RaBe substandard show that our PuBe source grows 0.80 ±0.18% per year.)

Some of the neutrons produced by the (p,n) reactions have energies above 1 MeV where the detector's response decreases with energy. To correct for the lower efficiency we deduced nuclear temperatures from published (p,n) spectra[12,13] for protons incident on ^{115}In and on the Sn isotopes and convolved the boil-off spectra with the efficiency curve. Curve e in Fig. 4 is the correction for ^{124}Sn; the other isotopes have higher thresholds and smaller corrections. We also corrected for counting losses using the deadtime determined from the observed counting rate versus beam current for a given target and proton energy. Uncertainties of ±20% of each of these corrections are included in the error bars. Room backgrounds were negligible except at low energies (curve d of Fig. 4).

C. Targets

We prepared targets by evaporation of Sn metal onto precision areas of nominal 14.2-mm diam on ^{58}Ni backings. The metal was enriched by the Isotopes Division at this laboratory. In the evaporation geometry the metal was held in a circular trough of the same diameter as the target on the axis at four diameters from the target. Targets produced in this geometry are highly uniform. Although the backings were mounted firmly behind a defining aperture, microscopic examinations showed each target to have an annular deposit about half the thickness of the central deposit and extending about 0.04-mm beyond the aperture

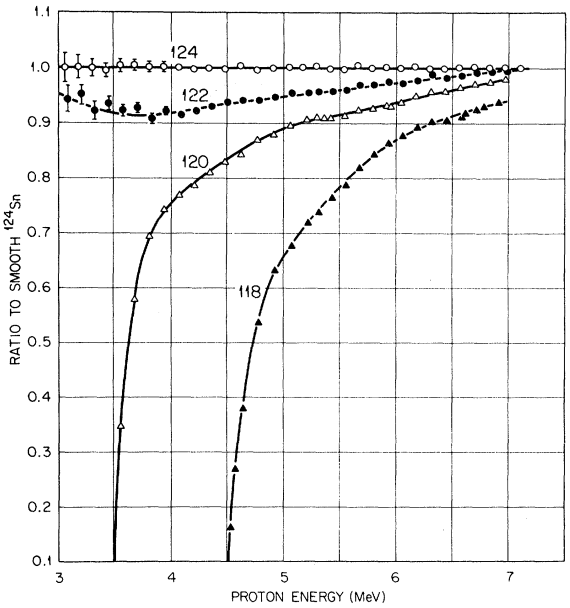

FIG. 2. Even Sn targets, ratios of the (p,n) cross sections to a smooth curve for ^{124}Sn(p,n). Interpolation is done with the empirical relation $\sigma \sim \exp(B/E)$.

limits. This was due to initial migration of the hot atoms. We assumed the area of the target to be that of the aperture but assigned a systematic ±0.3% uncertainty on the basis that half of the layer could have migrated to or from the aperture. We determined the weight of the deposit by weighing the backing on a microbalance, along with a standard, before and after evaporation. The backings were demagnetized to prevent interactions with the earth's field. The uncertainty in the weight of the deposit for all but ^{122}Sn was ±0.1%.

TABLE III. Random and systematic uncertainties in cross sections. The total systematic uncertainty combined in quadrature is < ±1%.

A. Included in Table II for individual points:	
(1) Counting statistics.	
(2) Energy reproducibility.	
(3) Deadtime corrections.	
(4) Background subtractions.	
(5) Transformation of $\bar{\sigma}$ to $\sigma(\bar{E})$.	
B. Systematic for a given target:	
(1) Areal density in Table I,	±0.1 to ±0.3 %.
(2) Isotopic corrections,	0.0 to ±0.2 %.
C. Systematic for all targets:	
(1) Absolute detector efficiency,	±0.6%.
(2) Absolute current integration,	±0.15%.
(3) Absolute proton energy, 3 MeV,	±0.35%.
4 MeV,	±0.25%.
>5.5 MeV,	±0.45%.
(4) Target edge effects	±0.3%.

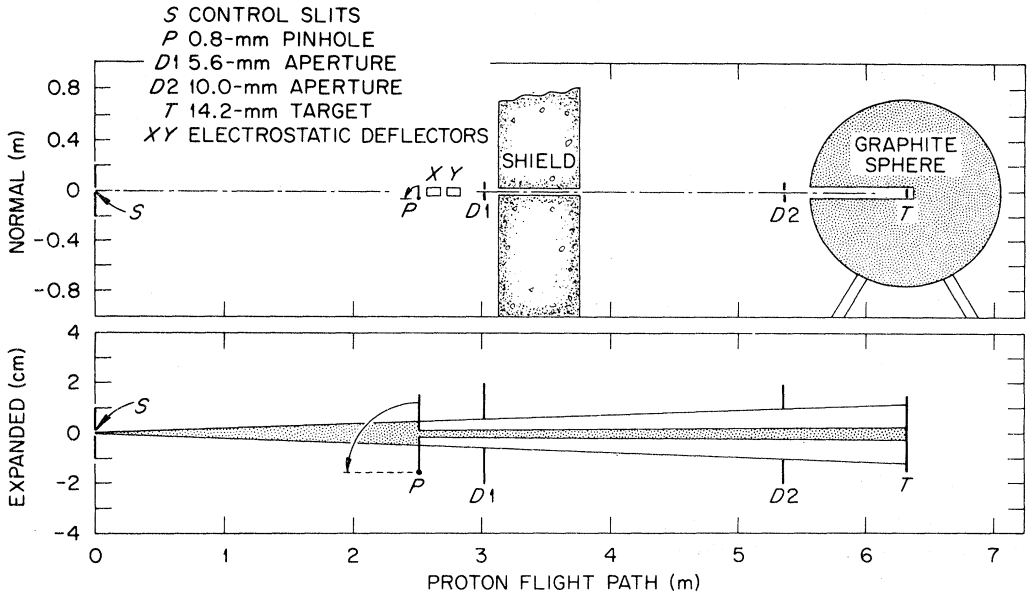

FIG. 3. Experimental geometry.

(For ^{122}Sn the uncertainty was larger, ±0.25%, because it was weighed without demagnetization.)

In the geometry of Fig. 3 the proton beam which emanates with small divergence from the control slits S is defined by aperture $D2$, but most of the excess beam is removed at $D1$ before the shield wall. The collimated beam irradiates two-thirds of the 14.2-mm diam target. We temporarily interposed the pinhole to produce a narrow beam to be used for scanning each target. From these scans we deduced the average areal density of the irradiated area relative to that of the total area and made corrections for nonuniformity ranging from 0.0 to 0.25%. The uncertainties in Table I include the errors in weight and one-half of this correction.

We corrected for (p,n) yields from the minor Sn isotopes in each target using our own measurements for ^{117,118,119,120,122,124}Sn and using cross sections for the other isotopes which are consistent with these data and with the known thresholds. For ^{116}Sn, which was 2.6% of the ^{117}Sn target, we included the analog-state resonance.[6]

D. Background from target contaminants

We minimized contaminants by cleaning the backings and by controlling the evaporations to minimize deposition of impurities. Nevertheless, there were contaminants with (p,n) yields. Corrections for neutrons produced in the backings, probably from ~0.01% of ^{61}Ni, were large (curve a of Fig. 4), but the uncertainties were only 5% of the corrections, or less than ±0.25% in the cross sections, and are included in the error bars.

Chlorine is a common contaminant. We determined the ^{37}Cl in each target by comparing the yield observed above the ^{37}Cl(p,n) threshold at 1.65 MeV with the known cross sections.[14,15] The ^{37}Cl abundances ranged from 0.0 to 0.008 at%; curve c of Fig. 4 corresponds to 0.003%. We subtracted this yield using the ^{37}Cl(p,n) excitation function[15] and included an uncertainty of ±50% of the corrections in the error bars.

The targets contained copper. Semiquantitative analyses of the Sn isotopes before evaporation

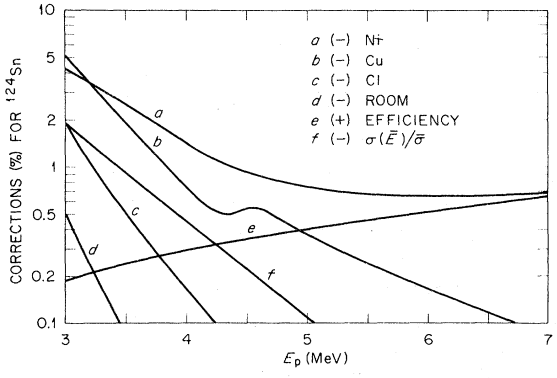

FIG. 4. Corrections to the observed ^{124}Sn(p,n) yields. Corrections a to d are background subtractions, correction e is for counting losses at high neutron energies, and f is for the nonlinear excitation functions. The sign of each is shown. Not shown are deadtime and minor-isotope corrections. Similar corrections were made for the other targets.

showed atomic abundances ranging from 0.02 to 0.06%. Since Cu and Sn have similar vapor pressures, we assumed the same abundances in the targets and subtracted background on the basis of known[16] Cu(p,n) cross sections. Independently we deduced the abundances from the observed yields near the 2.17-MeV threshold for ^{65}Cu(p,n) and found good agreement with the spectroscopic analyses, especially for those Sn targets with (p,n) thresholds above 2.17 MeV. Curve b in Fig. 4 corresponds to 0.06% of Cu. Uncertainties of ±50% of the corrections have been included in the error bars and are easily seen on the points below 4 MeV in Figs. 1 and 2. These uncertainties are the largest of the experiment.

IV. STRENGTH FUNCTIONS

Aside from threshold effects the dominant feature of each excitation function is the strong energy dependence due to penetration of the Coulomb barrier. But the nuclear effects can be revealed by dividing out the penetration factors. Given a proton total reaction cross section $\langle\sigma_r\rangle$ averaged over closely spaced resonances, an average strength function is reasonably defined[1] by

$$\langle S_p\rangle = R\frac{\langle\sigma_r\rangle}{4\pi^2k^{-2}\sum_l(2l+1)P_l}\,, \tag{1}$$

where P_l is the usual Coulomb penetration factor for l-wave protons at radius $R=1.45A^{1/3}$. Each observed cross section is $\langle\sigma_{p,n}\rangle$ rather than $\langle\sigma_r\rangle$. We define an experimental strength function

$$\langle S_{p,n}\rangle = R\frac{\langle\sigma_{p,n}\rangle}{4\pi^2k^{-2}\sum_l(2l+1)P_l}\,. \tag{2}$$

The $\langle S_p\rangle$ and $\langle S_{p,n}\rangle$ differ when protons and γ rays compete appreciably with neutron decay of the compound nucleus.

Corrections for these other decay modes are discussed in Sec. VI but Fig. 5 shows the experimental $\langle S_{p,n}\rangle$ deduced by visual fitting of the data in Figs. 1 and 2, with omission of the analog-state resonances. The dashed portions obviously must be corrected for γ-ray emission. Except for those portions the functions show striking systematic trends. Each shows a broad resonance. The resonant peaks indicated by arrows shift upward in energy with decreasing A. There are no observable odd-even effects; in fact, the small spacing between the peaks for ^{119}Sn and ^{120}Sn is consistent with $\Delta A=1$ for this pair. It appears that the ^{118}Sn function, corrected for γ-ray and proton emission, would fall in order between ^{117}Sn and ^{119}Sn. At 7 MeV the curves are in exact isotopic sequence, except for ^{118}Sn.

The $\langle S_p\rangle$ functions in Fig. 5 were predicted[1] from earlier data below 5.3 MeV with the requirement for consistency with proton scattering at higher energies. The upper arrows show the predicted peak energies. The difference between the observed and predicted resonant spacings is discussed in Sec. VIII.

V. OPTICAL MODEL AND ITS PARAMETER SPACE

The observed resonance in the strength function for a given isotope, with corrections for γ-ray emission, can be interpreted in terms of the broad quasibound $3p$ state in the proton optical model potential. The model used here is the usual form for low energies and is a sum of Woods-Saxon, surface absorptive, spin-orbit, and Coulomb potentials:

$$V(r) = -V_R f(r,R_R,a_R) + i4a_D W_D \frac{d}{dr} f(r,R_D,a_D) + V_{so}\frac{\vec{\sigma}\cdot\vec{l}}{r}\left(\frac{\hbar}{m_\pi c}\right)^2\frac{d}{dr}f(r,R_{so},a_{so}) + V_C(R_C)\,, \tag{3}$$

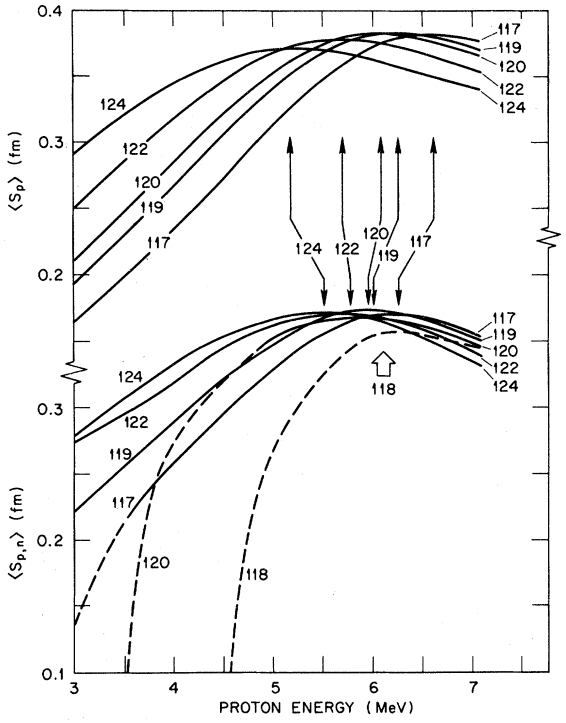

FIG. 5. Observed and predicted strength functions. The lower curves are visual fits to the data of Figs. 1 and 2 with the isobaric analog resonances omitted. Dashed portions have obvious threshold effects. The upper curves are optical-model predictions based on earlier data below 5.3 MeV and assumed continuity with scattering at 10 MeV and above (Ref. 1). Arrows indicate observed and predicted resonant maxima.

where

$$f(r,R,a)=\left[1+\exp\left(\frac{r-R}{a}\right)\right]^{-1}$$

and $R_x = r_x A^{1/3}$. The volume integrals of the first two terms are

$$J_R = \frac{4\pi}{3} R_R{}^3 V_R[1+(\pi a_R/R_R)^2] \quad (4)$$

and

$$J_D = 16\pi R_D{}^2 a_D W_D[1+\tfrac{1}{3}(\pi a_D/R_D)^2]. \quad (5)$$

The strength of the real local potential is energy dependent;

$$V_R(E) = V_R(0) - b_0 E. \quad (6)$$

We assume the absorptive potential is independent of energy because its total volume for protons from 10 to 60 MeV is found[17] to be constant even though the potential gradually changes from the surface to the interior at higher energies.

The Coulomb potential is known. A uniformly charged sphere of charge Ze and radius R_C is valid[18] providing R_C gives the same rms radius as the actual charge distribution. The charge radii for the Sn isotopes are known[19] and given by

$$R_C = [1.21+0.01(124-A)/6]A^{1/3}, \quad (7)$$

which corresponds to an $A^{1/6}$ dependence.

The data were fitted using the optical-model program GENOA[20] modified[21] to ensure a precision of ±0.1% in the absorption cross sections predicted at these energies below the barrier. Further modifications for γ-ray and proton emission are discussed below. The program varies the parameters to minimize the function

$$\chi^2 = \frac{1}{N}\sum_1^N \left(\frac{\sigma_{\rm exp}-\sigma_{\rm th}}{\sigma_{\rm error}}\right)^2, \quad (8)$$

where N is the number of data, $\sigma_{\rm exp}$ and $\sigma_{\rm th}$ are the experimental and theoretical cross sections, respectively, and $\sigma_{\rm error}$ is the experimental uncertainty.

This 10-parameter model is overparametrized for the present data because each excitation function, corrected for γ-ray and proton emission, warrants only three parameters to fit the energy, width, and height of the resonance. We begin by fixing the spin-orbit potential with parameters (Table IV) from an analysis[22] of scattering and polarization at 9.8 MeV. The spin-orbit potential broadens the resonance slightly by introducing a $p_{1/2}$-$p_{3/2}$ splitting of about 0.5 MeV.

The model is thereby reduced to seven parameters of which four must be fixed. For reasons discussed below we fix r_R, a_R, b_0, and r_D at the values listed in Table IV. The remaining free variables are W_D, a_D, and $V_R(0)$; in effect, W_D and a_D are used to fit the height and width of the resonance and $V_R(0)$ is used to fit the energy. The essential quantity for the resonant energy is VR^2 calculated for the real well at the resonance. We abbreviate this by P_R.

TABLE IV. Fixed proton optical-model parameters.

V_{so} (MeV)	r_{so} (fm)	a_{so} (fm)	r_R (fm)	a_R (fm)	b_0 (MeV^{-1})	r_D (fm)
6.4	1.03	0.63	1.2	0.73	0.32	1.3

We studied the parameter space by making repeated least-squares analyses of the observed ^{124}Sn(p,n) cross sections using various values of the normally "fixed" parameters. For this target, $\langle S_p\rangle \simeq \langle S_{p,n}\rangle$ because the threshold is low and the residual odd-odd nucleus has many levels. Figure 6 demonstrates the sensitivity of χ^2 to each of the three free parameters. Zero deviation corresponds to the best-fit values. To obtain each curve we gridded the indicated parameter over a range of fixed values while searching on the remaining two. With the above fixed parameters, the real depth is determined to better than ±0.1%, and W_D and a_D each to about ±2%.

Figures 7(a) to 7(d) show the effects of changing the "fixed" parameters. For each figure three of the fixed parameters were held to the values in Table IV while the fourth was gridded along the abscissa. The vertical lines correspond to the above best fit and the curves show the percentage deviations of P_R, J_D, and a_D for repeated best fits. The indicated variations in χ^2 are small except for the outer regions in b_0. The following discussion includes the reasons for choosing the fixed values.

The radius r_D. Figure 7(a) shows that variations

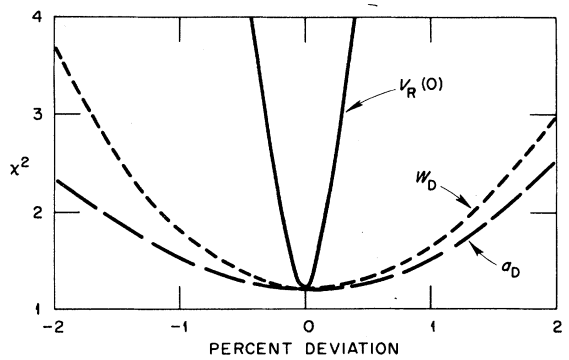

FIG. 6. Sensitivity of χ^2 to each of the three free parameters, $V_R(0)$, W_D, and a_D. In these curves, which were obtained by fitting ^{124}Sn(p,n), the abscissa is the deviation of the indicated parameter from its best-fit value and the ordinate is the minimum χ^2 obtained by readjustment of the other two free parameters.

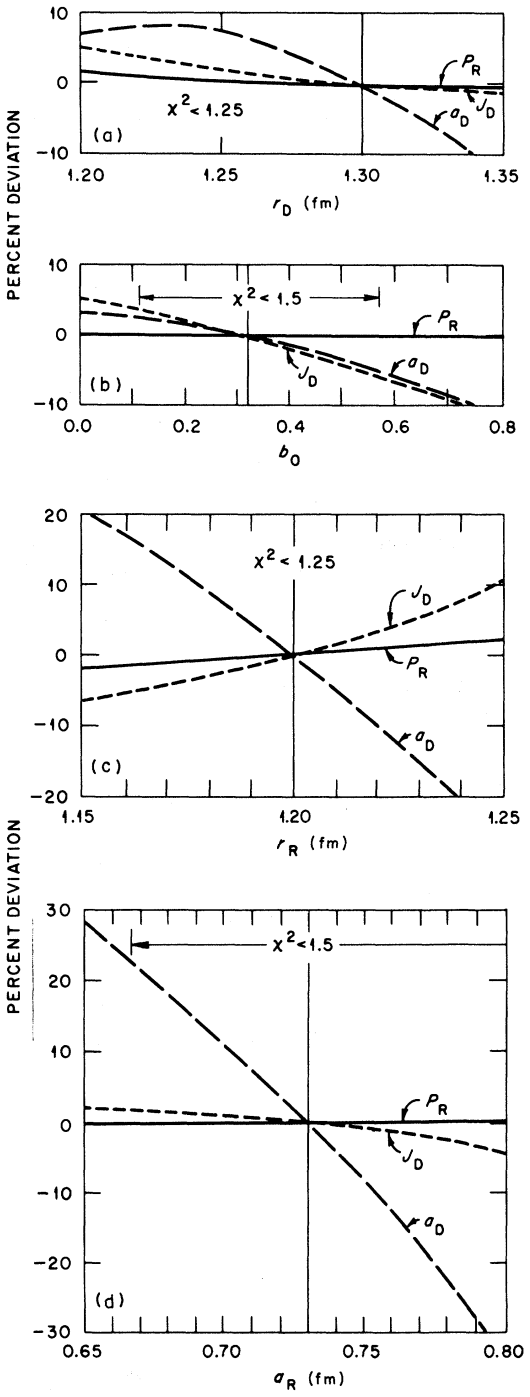

FIG. 7. Investigation of the fixed-parameter space for the proton optical model. The curves were obtained by fitting ^{124}Sn(p,n). In each figure the vertical line corresponds to the normally fixed values of r_D, b_0, r_R, and a_R in Table IV, and the curves show the variation in the best-fit values of a_D, J_D, and P_R for changes in the fixed parameter indicated by the abscissa. (P_R is an abbreviation for VR^2 for the real well at the resonant peak in $\langle S_p \rangle$.) The small variations in χ^2 are indicated.

in r_D over a reasonable range give equally good fits to the data with adjustments of about 1% in P_R, 5% in J_D, and 20% in a_D. Clearly r_D is not sensitive and could not replace a_D as one of the two absorptive-potential variables needed to fit the height and width of the resonance. The fixed value, $r_D = 1.3$ fm, is consistent with an analysis by Becchetti and Greenlees[18] at higher energies.

The energy coefficient b_0. Increasing the energy dependence in the real local potential introduces a level shift which broadens the $3p$ resonance. Figure 7(b) shows that this broadening can be compensated by decreasing a_D. The resonant condition P_R remains constant and the required adjustments in the strength W_D are small. Of the four "fixed" parameters, only b_0 gives a definite broad minimum in χ^2. The fixed value, $b_0 = 0.32$ MeV^{-1}, was chosen from Becchetti and Greenlees, but it also gives the χ^2 minimum for ^{124}Sn. Section VIII has further justifications for this b_0.

Geometry of the real potential. Figures 7(c) and 7(d) show that a change in either r_D or a_R for the real well can be compensated by a change of the opposite sign in the absorptive diffuseness a_D; further adjustments in the strengths are needed to maintain J_D and P_R essentially constant. Approximately, $\partial a_D/\partial a_R = -1.7$ and $\partial a_D/\partial r_R = -2$. From a phenomenological viewpoint, either term in the real geometry could replace a_D as one of the free parameters; however, Greenlees *et al.*[23,24] have shown that the rms radius is well defined, independent of proton energy, and related to the actual rms mass radius of the nucleus. From scattering and polarization data Boyd *et al.*[25] deduced the rms radii to ±0.1 fm for the even Sn nuclei. The corresponding uncertainty in the optical-model geometry is $\Delta a_R = \pm 0.05$ fm for fixed r_R or $\Delta r_R = \pm 0.03$ fm for fixed a_R. Since Figs. 7(c) and 7(d) show these limits to be equivalent to about ±20% in a_D, the replacement of the variable a_D by a_R or r_R would not suffice unless a_D were initially chosen properly to ±20%. We chose the fixed geometry in Table IV to give a good representation of the average rms radii[25] for an assumed $A^{1/3}$ dependence in R_R. In Fig. 8 the vertical line corresponds to this choice and the curves show variations in the best-fit a_D, J_D, P_R, and the corresponding χ^2 for a constant rms radius but various geometries. The fixed geometry gives the minimum χ^2 for ^{124}Sn and is consistent with analyses[18,22,26] of scattering and polarization at higher energies.

Summary. Figures 7 and 8 show that a_D and W_D are the proper free parameters for the absorptive potential and that the proper parameter for the real potential is the strength of the potential at the resonance or, more precisely, VR^2 at the reso-

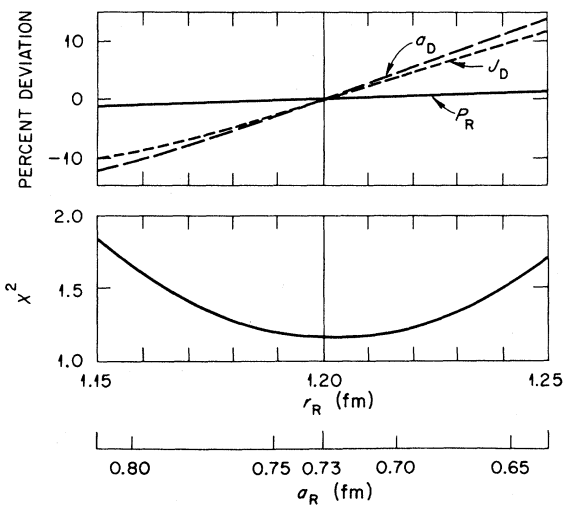

FIG. 8. Sensitivity to the geometry of the real well for a fixed rms radius. The curves were obtained by fitting ^{124}Sn(p,n). (See Fig. 7.) All points on the abscissa correspond to a given rms radius.

nance energy with limits on R_R. The range of values plotted for r_D and b_0 are reasonable limits and the known rms radii place some limits on the real geometry. The resulting overall uncertainties propagated from ambiguities in the "fixed" parameters are about ±30% in a_D, ±4% in J_D, and ±1% in VR^2 for the real well at the resonant energy. Clearly the present data can reveal the isotopic dependence in VR^2 at the resonance, and possibly in J_D, but an apparent dependence for the absorptive diffuseness a_D could be reinterpreted, at least in part, in terms of the geometry of the real potential.

VI. CORRECTIONS FOR γ-RAY AND PROTON EMISSION

A. Statistical model

According to the statistical theory of nuclear reactions[27] incident protons of energy E_p in channel Jsl form states of J^π at excitation E_x which decay independently of the entrance channel. The (p,n) cross section averaged over closely spaced resonances is given by

$$\langle\sigma_{p,n}\rangle = \sum_{Jsl}\langle\sigma_r\,\Gamma_n/\Gamma\rangle_{Jsl} = \sum_{Jsl}\langle\sigma_r\rangle_{Jsl}\,\theta_{Jsl}\left(1+\frac{\langle\Gamma_p\rangle}{\langle\Gamma_n\rangle}+\frac{\langle\Gamma_\gamma^*\rangle}{\langle\Gamma_n\rangle}\right)^{-1}_{Jsl}, \quad (9)$$

where $\langle\Gamma_p\rangle_{Jsl}$, $\langle\Gamma_\gamma^*\rangle_{Jsl}$, and $\langle\Gamma_n\rangle_{Jsl}$ are proton, γ-ray, and neutron decay widths averaged over the compound states and summed over final states that are accessible in the respective target, compound, and final nuclei. The asterisk notation, $\langle\Gamma_\gamma^*\rangle$ and also $T^*_{\gamma J\pi}(E_x)$, indicates the exclusion of radiation to states that cascade by neutron emission and appear in the neutron yield. The fluctuation[28] factor θ_{Jsl} allows the average of a product to be replaced by individual averages.

It is convenient to define an overall ratio of neutron and total widths

$$\frac{\Gamma_{nT}}{\Gamma} \equiv \frac{\langle\sigma_{p,n}\rangle}{\langle\sigma_r\rangle}. \quad (10)$$

Since uncertainties in the input data for the statistical model preclude accurate predictions, we introduce as much information as seems reasonable but leave one or two parameters free. We then make least-squares fits using the theoretical expression

$$\sigma_{p,n} = \frac{\Gamma_{nT}}{\Gamma}\langle\sigma_r\rangle, \quad (11)$$

where $\langle\sigma_r\rangle$ is calculated from the proton optical model with its adjustable parameters and Γ_{nT}/Γ is calculated from the statistical model with its additional parameters.

This ratio is not sensitive to the parameters of the proton potential. The potential determines the initial distribution in J^π of compound states and gives the transmission factors for proton reemission to the target. We use a potential consistent with the results of the present paper. The low-lying target states are well known,[29-33] so the small proton reemission is calculated with little uncertainty.

The central problem is to calculate the ratio of γ ray to neutron widths which is given by

$$\frac{\langle\Gamma_\gamma^*(E_x)\rangle_{J\pi}}{\langle\Gamma_n(E_x)\rangle_{J\pi}} = \frac{T^*_{\gamma J\pi}(E_x)}{\sum_{\epsilon J's'l'} T_{l'}(E_n) + \int_{E_1}^{E_2}\sum_{J's'l'} T_{l'}(E_n)\rho_{J'\pi'}(\epsilon)\,d\epsilon}. \quad (12)$$

The denominator includes neutron optical-model transmission factors summed over the known states of excitation $\epsilon < E_1$ in the residual nucleus and integrated over the continuum of states of density $\rho_{J'\pi'}(\epsilon)$ from E_1 to the maximum E_2 corresponding to $E_n = 0$. (These transitions must obey the conservation laws.) The numerator is given by

$$T^*_{\gamma J\pi}(E_x) = 2\pi\rho_{J\pi}(E_x)\langle\Gamma_\gamma^*(E_x)\rangle_{J\pi} \quad (13)$$

and may be called a "γ-ray transmission factor." (The γ-n cascades that are omitted from the numerator make a negligible addition to the denominator.)

B. Neutron data for the statistical model

Neutron transmission factors are relatively certain. We use typical optical-model param-

eters[34] with the spin-orbit term omitted. Neutrons populate the known low-lying states in the residual nucleus and the unknown continuum above those states. The Appendix includes our evaluation of the literature on levels below 2 MeV in the residual odd-even nuclei ^{117,119}Sb. The uncertainties in these structures are negligible for the present work. The levels of the residual odd-odd nuclei have been partially observed by (p,n) reactions but are still poorly known. The Appendix includes the available data below 1200 keV in ^{118,120}Sb and below 500 keV in ^{122}Sb. It also includes speculative J^π assignments which are only intended to be used for the above sum over states. The continuum is an extrapolation normalized to the density of low-lying states. It becomes less certain at higher energies but also less important because the upper continuum is populated only at proton energies well above threshold where nearly all of the decay is by neutron emission.

C. Level densities

A density formula is required for extrapolating into the continuum of the residual nucleus and for calculating γ-ray transmission factors in the compound nucleus. Nuclear level densities have been discussed by many authors.[35] For the total density at excitation energy $U = E_x - \Delta$, measured from a fictive ground state Δ, we use

$$\rho(U) = \frac{\exp[2(aU)^{1/2}]}{12\sqrt{2}\,\sigma a^{1/4} U^{5/4}} . \tag{14}$$

For the spin-dependent density, including both parities, we use

$$\rho_J(U) = \rho(U)\{\exp(-J^2/2\sigma^2) - \exp[-(J+1)^2/2\sigma^2]\}, \tag{15}$$

where σ and a are the spin cutoff and density parameters. The spin cutoff is not too critical because the targets have low spins and the available high-spin states of the compound and final nuclei are limited by the neutron and proton centrifugal barriers. We use the expression[36] $\sigma^2 = 0.0888(aU)^{1/2}A^{2/3}$. This corresponds, for the Sn and Sb nuclei and for $a = 15$, to about 75% of the rigid body moment of inertia.

The density formula has two parameters, Δ and a, which are often adjusted[37] to fit both the density observed near the ground state and the density of states with specific J observed by scattering of s-wave neutrons near the separation energy. In the present case the total density of low-lying states is essentially known for each Sb nuclei of interest, $117 \leq A \leq 123$, but resonances at the neutron separation energies have been observed only for ^{122,124}Sb because only ^{121,123}Sb are stable. However, Dilg *et al.*[37] found for this mass region that a is nearly constant, about 15 ± 1 MeV^{-1}, and independent of odd-even effects. Therefore, we use $a = 15$ MeV^{-1} and normalize Δ to the low-lying states as discussed in the Appendix. This is consistent for ^{122}Sb because the predicted spacing of 2^+ and 3^+ levels at the neutron separation energy is then 9 eV, in agreement with the observed[38] 10.3 ± 1 eV.

D. Radiative widths

Average radiative widths of about 100 meV have been observed[38] for resonances near the neutron separation energy in this mass region, but data are not available for the Sb nuclei of primary interest here or for the higher excitations. It is reasonable to use the γ-ray dipole strength function[39] to predict radiative widths. For decay of levels of given J^π at energy E_x to a specific final state i at energy $E_x - E_\gamma$ the strength function is defined by

$$f(E_\gamma) = \rho_J(E_x - \Delta)\Gamma_{\gamma i J}(E_x)/E_\gamma{}^3 \tag{16}$$

and is assumed to be independent of J. An estimate of $f(E_\gamma)$ is obtained by assuming[40,41] that the tail of the $E1$ giant dipole resonance determines the energy dependence at lower γ-ray energies;

$$f(E_\gamma) = \frac{26\times10^{-8}}{3}\ \frac{\sigma_g \Gamma_g{}^2 E_\gamma}{(E_\gamma{}^2 - E_g{}^2)^2 + (\Gamma_g \Gamma_\gamma)^2} , \tag{17}$$

where E_g and Γ_g are the dipole resonant energy and width, respectively, in MeV, and σ_g is the peak photoabsorption cross section in mb. The total radiative width, excluding γ-n cascades and averaged over initial states of J^π, is found by summing over spins of final states populated by electric dipole radiation and integrating from an appropriate γ-n threshold to the maximum γ-ray energy:

$$\langle \Gamma_\gamma^*(E_x)\rangle_{J\pi} = \int_{E_p - E_c}^{E_x} \frac{f(E_\gamma)E_\gamma{}^3}{\rho_J(E_x - \Delta)} \times \sum_{I=J-1}^{I=J+1} \rho(E_x - E_\gamma - \Delta)\,dE_\gamma . \tag{18}$$

A reasonable estimate of E_c is the proton energy near threshold where $\langle\sigma_{p,n}\rangle/\langle\sigma_r\rangle = 0.5$. This energy is about 0.1 MeV above threshold for the even targets and about 0.5 MeV for the odd ones.

The level density $\rho_J(U)$ cancels when this integral is substituted into Eq. (13) but the results are understood better by keeping $\rho_J(U)$ in the integral. If we had assumed a density $\sim\exp(E_x/t)$ with constant temperature t, the total radiative width would have been nearly independent of energy and slowly decreasing with J. Approximately, for large J,

$$\langle\Gamma_\gamma(E_x)\rangle_{J\pi} = 4!\,(26\times10^{-8})\sigma_g\,\Gamma_g^2 t^5/E_g^4\,, \qquad (19)$$

but for the assumed Fermi gas distribution the nuclear temperature is energy dependent and the radiative width varies approximately as $U^{5/2}$.

Bartholomew *et al.*[39] concluded from experimental data on photoabsorption and radiative capture that $E_g = 15.2$ MeV, $\Gamma_g = 4.5$ MeV, and $\sigma_g = 254$ mb for Sb; but for the above density parameters σ_g must be reduced to 160 mb to predict radiative widths consistent with the observed[38] 100 meV in ^{122,124}Sb. For the following predictions we use an average, $\sigma_g = 210$ mb.

E. Statistical model predictions of $\langle\sigma_{p,n}\rangle/\langle\sigma_r\rangle$

We wrote a statistical-model computer code separate from the optical-model search routine. Figure 9 shows curves predicted from the input data discussed above and in the Appendix. Odd-even effects are apparent; the ^{117}Sn and ^{122}Sn curves are different even though the thresholds are similar; the same is true for ^{119}Sn and ^{124}Sn. Generally, proton reemission is much less than 1% of the total; the largest value predicted is 1.2% for 7-MeV protons on ^{119}Sn.

F. Adjustable parameters for the statistical model

The adjustable parameters should be related to the data of the statistical model that have the largest uncertainties. Both the neutron and γ-ray data include the level density parameters; however, for γ rays these are used for long and critical extrapolations into unexplored regions of the compound nucleus whereas, for neutrons, they are used for relatively short and noncritical extrapolations from the observed density of low-lying states. We decided to adjust the γ-ray transmission factors while leaving the neutron data fixed as above.

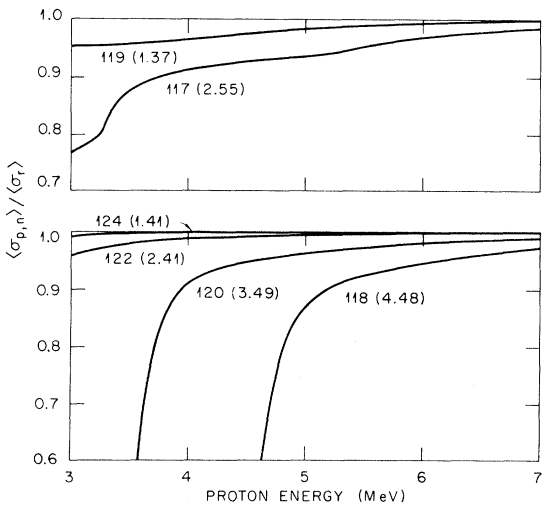

FIG. 9. Statistical model predictions of $\langle\sigma_{p,n}\rangle/\langle\sigma_r\rangle$ for isotopes of Sn. The curves are labeled by the atomic weight and, in parentheses, the (p,n) threshold in MeV. Data for the predictions are in Table V, the text, and the Appendix.

For this parametrization it is convenient to factor the computed γ-ray transmissions as follows:

$$T^*_{\gamma J\pi}(E_x) = C(E_p - E_c)I(J,\sigma)T_{\gamma 0}(E_x)\,. \qquad (20)$$

The γ-n cascade function $C(E_p - E_c)$ defined here is unity up to a proton energy E_c and decreases slowly above that. The smallest value predicted above is 0.4 for 7-MeV protons on ^{119}Sn, and it is not critical in any case. The spin function $I(J,\sigma)$ is defined here to include the J dependence in the level density and a small J dependence predicted for Γ_γ. In the following we retain the functions C and I calculated above.

The transmission factor $T_{\gamma 0}(E_x)$ can be factored further into constant and energy-dependent terms:

$$T_{\gamma 0}(E_x) = T_{\gamma 0}(E_0)(U/U_0)^{1/2}\exp[2\sqrt{a}\,(\sqrt{U} - \sqrt{U_0})]\,, \qquad (21)$$

where $U = E_x - \Delta$, $U_0 = E_0 - \Delta$, and $T_{\gamma 0}(E_0)$ is the transmission factor, including γ-n cascades, for compound states of $J = 0$ at an excitation E_0 corresponding to an appropriate proton energy for each (p,n) curve. The $U^{1/2}$ term comes from the U^{-2} dependence in the level density and the approximate $U^{5/2}$ dependence predicted in Γ_γ.

An energy derivative is also useful. We define D_x

$$D_x = \frac{d}{d\sqrt{E_x}}\ln[T_{\gamma 0}(E_x)] \simeq 2\sqrt{a}\,. \qquad (22)$$

It is related to the familiar nuclear temperature t

$$\frac{1}{t} = \frac{d}{dU}\ln[\rho(U)] = (a/U)^{1/2} - 3/2U\,. \qquad (23)$$

Both D_x and t^{-1} are roughly proportional to $\sqrt{a}$.

Both the constant $T_{\gamma 0}(E_0)$ and the derivative D_x are used below as adjustable parameters. For reference, Table V lists values predicted above for the curves in Fig. 9. The $T_{\gamma 0}(E_0)$ are proportional to $\exp[2(aU_0)^{1/2}]$ and approximately to $\sigma_g\Gamma_g^2/E_g^4$. Also in the table are values for slow neutrons incident on stable Sb nuclei. These are included to emphasize the long extrapolations from the known neutron resonant spacings and radiative widths to the present data and to show that renormalization of $T_{\gamma 0}(E_0)$ is reasonable.

TABLE V. Statistical model predictions of γ-ray transmission factors for $\sigma_g = 210$ mb, $\Gamma_g = 4.5$ MeV, $E_g = 15.2$ MeV, and $a = 15$ MeV^{-1}. The fictive ground state Δ is for the compound nucleus. The compound excitation energy E_0 corresponds to proton or neutron energy E_p or E_n.

Reaction	Δ (MeV)	E_p or E_n (MeV)	E_0 (MeV)	$T_{\gamma 0}(E_0)$	D_x (MeV$^{-1/2}$)	$t(E_0)$ (MeV)
^{117}Sn+p	−0.5	3.0	7.82	0.025	7.88	0.86
^{118}Sn+p	+0.7	5.0	10.08	0.104	8.37	0.90
^{119}Sn+p	−0.5	3.0	8.62	0.072	7.94	0.89
^{120}Sn+p	+0.7	4.0	9.52	0.066	8.37	0.88
^{122}Sn+p	+0.7	3.0	9.55	0.044	8.37	0.88
^{121}Sb+n	−0.9	0.0	6.81	0.0098		0.83
^{123}Sb+n	−0.95	0.0	6.47	0.0065		0.82

VII. ANALYSES OF THE EXPERIMENTAL STRENGTH FUNCTIONS

A. Assumption of $\langle S_p \rangle = \langle S_{p,n} \rangle$

The statistical model predictions in Fig. 9 indicate that the (p,n) cross sections observed above 3 MeV for ^{119}Sn, ^{122}Sn, and ^{124}Sn are nearly $\langle \sigma_r \rangle$.

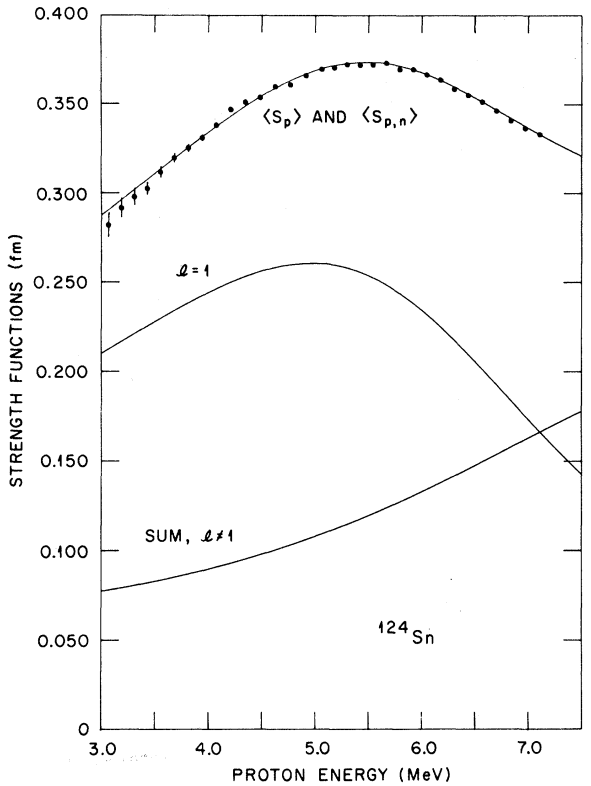

FIG. 10. Three-parameter optical-model fit to ^{124}Sn(p,n). The points are experimental strength functions $\langle S_{p,n} \rangle$. The fitted curve is $\langle S_p \rangle$ for parameters from Tables IV and VI. An almost identical curve would be given by the global parameters of Tables IV and VII. The lower two curves are the partial-wave contributions which add to give $\langle S_p \rangle$. The actual partial p-wave function s_1, as defined in Ref. 1, has a 0.65-fm peak at 0.2 MeV below the peak for $\langle S_p \rangle$.

Assuming $\langle S_p \rangle = \langle S_{p,n} \rangle$, we fit each of these three by least-squares adjustments of $V_R(0)$, W_D, and a_D, with the other parameters fixed (Table IV). Figures 10 and 11 show the fits and Table VI lists χ^2, the parameters, and the volume integrals per nucleon. Figure 10 includes the partial-wave contributions that add together to give $\langle S_p \rangle$. *Deductions about the optical model that might have been made solely from these fits with neglect of γ-ray emission would have differed little from final global analysis below.* The parameters are nearly the same as for the global analysis except that the

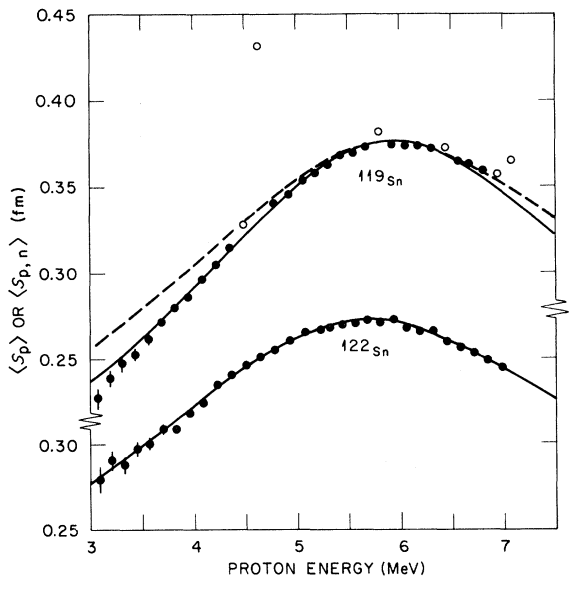

FIG. 11. Strength functions for ^{119,122}Sn. Data points are the observed $\langle S_{p,n} \rangle$; open symbols near analog-state resonances are data omitted from the search. Solid curves are the fitted $\langle S_p \rangle$ for parameters in Tables IV and VI. Dashed curve is $\langle S_p \rangle$ for global parameters in Tables IV and VII. Not shown are global fitted $\langle S_{p,n} \rangle$; they are similar to the solid curves except above the ^{119}Sn peak where the dashed curve is closer to the global $\langle S_{p,n} \rangle$.

TABLE VI. Optical-model parameters deduced from ^{119,122,124}Sn(p,n), assuming $\langle S_{p,n}\rangle = \langle S_p\rangle$.

Target	χ^2	$V_R(0)$ (MeV)	W_D (MeV)	a_D (fm)	J_R/A [a] (MeV fm^3)	J_D/A (MeV fm^3)
^{119}Sn	2.3	63.58	11.59	0.352 [b]	514.1	71.2
^{122}Sn	1.9	63.43	11.46	0.417	512.7	83.0
^{124}Sn	1.2	63.53	10.92	0.419	513.4	79.0

[a] Calculated at the energy of the maximum for the partial strength function s_l for p waves. [See Eq. (4) of Ref. 1 for definition of s_l].

[b] The low value of a_D results because the approximation $\langle S_{p,n}\rangle = \langle S_p\rangle$ is not good enough for ^{119}Sn(p,n).

diffuseness a_D for ^{119}Sn is about 10% smaller here; comparisons with the global fit (dashed curve in Fig. 11) show that the smaller a_D is an erroneous result from the assumption $\langle S_{p,n}\rangle = \langle S_p\rangle$, which is only approximate for ^{119}Sn.

B. Attempt to renormalize $T_{\gamma 0}(E_0)$ for individual targets

Since γ-ray emission is not quite negligible for ^{119}Sn, and certainly not for ^{117,118,120}Sn, we fitted each of these with the combined statistical-optical-model search routine using $T_{\gamma 0}(E_0)$ as a fourth parameter. Since the experimental level density parameters in this mass region have a limited range of values,[37] approximately $13 \leq a \leq 16$, corresponding to fairly well defined nuclear temperatures, we had anticipated that renormalization of $T_{\gamma 0}(E_0)$ at an energy E_0 near threshold where γ-ray emission is important would allow extrapolations upward without adjustments of the energy derivatives. Even though the fits were acceptable, we conclude that the parameters are not physically realistic. Figure 12(a) shows the $\langle S_p\rangle$ predicted from the fits for these four targets along with the above curves for ^{122}Sn and ^{124}Sn. Obviously for ^{118}Sn the optical model has been erroneously adjusted to fit the data near the 4.5-MeV threshold. The models for ^{117,119,120}Sn appear to be erroneously adjusted but more subtly so; the predicted resonances in $\langle S_p\rangle$ for these three do not shift upward in energy with decreasing A, as expected from the optical model and as observed for ^{122}Sn and ^{124}Sn, but remain at the same energy and grow in amplitude. Thus, according to this analysis, the observed systematic trend in the peaks shown in

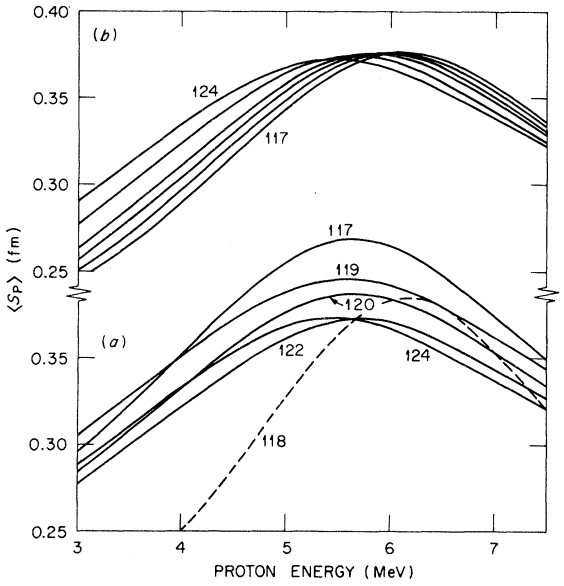

FIG. 12. (a) Unsystematic $\langle S_p\rangle$ from individual four-parameter analyses, except ^{122,124}Sn. Curves for ^{122,124}Sn are for $\langle S_p\rangle$ from Figs. 10 and 11. The curves for ^{117,118,119,120}Sn are $\langle S_p\rangle$ deduced by four-parameter analyses including adjustable $T_{\gamma 0}(E_0)$. (b) Predicted $\langle S_p\rangle$ from global parameters of Tables IV and VII.

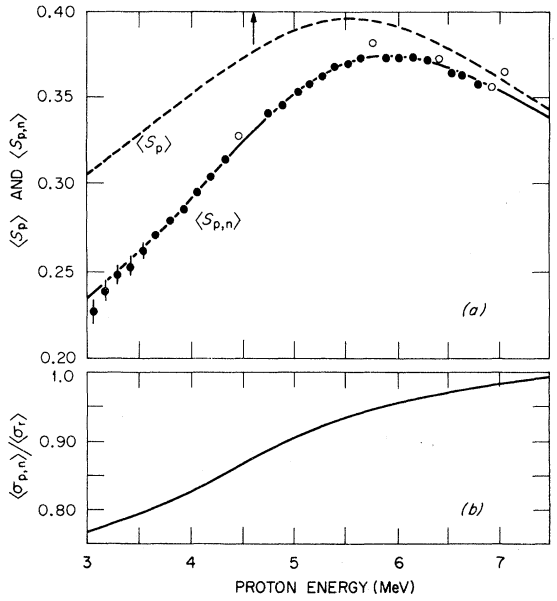

FIG. 13. Effects of γ-ray emission in four-parameter analysis of ^{119}Sn(p,n). Data are the same as in Fig. 11. The lower curve multiplied by $\langle S_p\rangle$ gives the fitted $\langle S_{p,n}\rangle$.

Fig. 5 results from a fortuitous cancellation of the effects of γ-ray emission and the strength functions.

This cancellation is demonstrated specifically for ^{119}Sn in Fig. 13. The points are the same as in Fig. 11 and the fit is not much different, but the interpretation is that a slowly rising $\langle\sigma_{p,n}\rangle/\langle\sigma_r\rangle$ (lower curve) is multiplied by an $\langle S_p\rangle$ (dashed curve) which is shifted down in energy and up in magnitude from the observed $\langle S_{p,n}\rangle$. The slow rise in $\langle\sigma_{p,n}\rangle/\langle\sigma_r\rangle$ results from the assumed nuclear temperatures.

C. Global analysis

In Fig. 12(a) above the deviations of $\langle S_p\rangle$ from the expected pattern for the proton optical model is not sufficient reason for discarding them because the model is expected to be good only on the average. Apparently no strong reasons exist, *a priori,* for the functions to be in exact isotopic sequence. Nevertheless, it is unreasonable that the deviations of $\langle S_p\rangle$ from the average optical model would just cancel the random threshold effects to produce the observed systematic trend in $\langle S_{p,n}\rangle$. Therefore, for the final analysis of all six targets *we assume that the observed systematic trend in* $\langle S_{p,n}\rangle$ *for the* Sn *isotopes results from a systematic isotopic dependence in the proton entrance channel rather than from compensating variations in* $\langle S_p\rangle$ *and* Γ_γ/Γ_n. To formulate this in terms of the optical model we add an adjustable isotopic term to each of its adjustable parameters;

$$V_R(0) = V_0 + V_\epsilon\epsilon\,,$$
$$W_D = W_0 + W_\epsilon\epsilon\,, \qquad (24)$$

and

$$a_D = a_0 + a_\epsilon\epsilon\,,$$

where

$$\epsilon = (N-Z)/A\,.$$

These expressions are analogous to those used at higher energies but may not have the significance of isospin dependences. (A small Coulomb correction[42] is implicit in $V_\epsilon\epsilon$.)

Since this assumption by itself is too restrictive for a global fit, we include the derivative D_x (Eq. 22) as an adjustable parameter. For proton energies within 1 or 2 MeV of threshold, where the neutrons populate mostly the residual discrete states, this is equivalent to adjusting the temperature of the compound nucleus. At higher energies it is equivalent to adjusting the difference in reciprocal temperatures for the compound and residual continua. Only two adjustable D_x parameters are introduced, one for the odd targets and another for the even ones. That restriction is not necessary but is reasonable. The normalization factor $T_{\gamma 0}(E_0)$ is also adjusted for each target except ^{124}Sn, for which γ-ray emission is negligible. The resulting total number of parameters is 13, an average of 2.2 per excitation function.

The corrections for γ-ray emission have the largest uncertainties for ^{118}Sn and ^{120}Sn because the thresholds are above 3 MeV and the residual states are poorly known. Therefore we reduced the weighting factors for these two by doubling the errors and discarding points within 200 keV of the thresholds.

We adjusted the 13 parameters by least squares to fit all six (p,n) excitation functions. Table VII lists the best-fit parameters and χ^2 for each target. Values of $T_{\gamma 0}(E_0)$ and D_x are given relative to the predictions in Table V. (The coefficients V_ϵ, W_ϵ, and a_ϵ are implicit in the systematic variations in $V_R(0)$, W_D, and a_D.) Included are the energies $E_{\max}$ predicted for the peaks in the partial p-wave strength functions and the values of J_R/A and VR^2 computed for the real well at $E_{\max}$. Each peak in $\langle S_p\rangle$ is about 0.2 MeV above $E_{\max}$. Values of J_D/A for the absorptive potential are listed.

Figure 14 shows the fitted curves for $\langle\sigma_{p,n}\rangle/\langle\sigma_r\rangle$

TABLE VII. Global parameters. [T_1 and D_1 are predicted $T_{\gamma 0}(E_0)$ and D_x in Table V].

A	χ^2	$\frac{T_{\gamma 0}(E_0)}{T_1}$	$\frac{D_x}{D_1}$	$V_R(0)$ (MeV)	W_D (MeV)	a_D (fm)	$E_{\max}$ [a] (MeV)	VR^2 [b] (MeV fm^2)	J_R/A [b] (MeV fm^3)	J_D/A (MeV fm^3)
117	1.4	2.73	0.39	63.48	11.82	0.385	6.05	2120	513.4	80.0
118	7.0 [c]	2.63	0.63	63.49	11.71	0.391	5.95	2134	513.5	80.2
119	0.5	2.95	0.39	63.50	11.60	0.397	5.85	2147	513.5	80.4
120	4.1 [c]	1.63	0.63	63.51	11.49	0.402	5.75	2160	513.5	80.6
122	3.2	1.17	0.63	63.53	11.27	0.413	5.50	2188	513.5	80.9
124	1.9			63.55	11.06	0.424	5.25	2215	513.6	81.1

[a] Energy of p-wave peak. The peak energy for $\langle S_p\rangle$ is $E_{\max}+0.2$ MeV for ^{124}Sn, and $E_{\max}+0.1$ MeV for ^{117}Sn. See footnote (a) of Table VI.

[b] Calculated at $E_{\max}$.

[c] Uncertainties in Table II multiplied by 2.

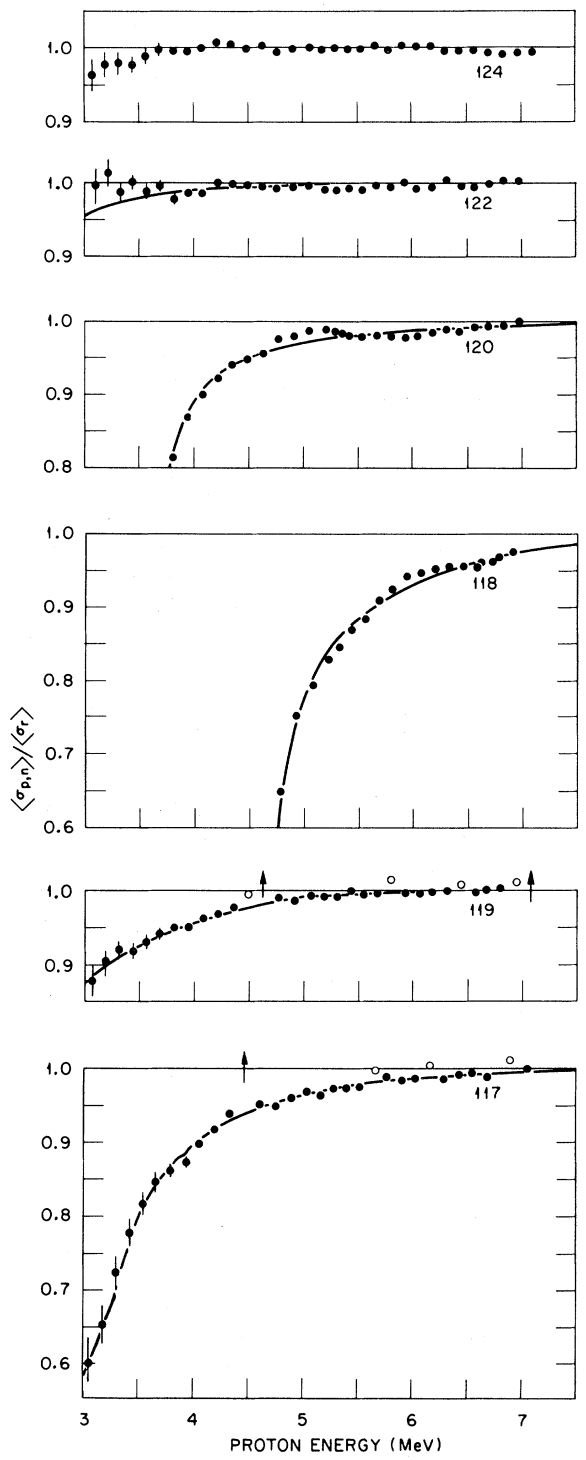

FIG. 14. Predicted $\langle\sigma_{p,n}\rangle/\langle\sigma_r\rangle$ from the global analysis. Fitted curves are calculated from optical-model parameters in Tables IV and VII and statistical-model parameters in Tables V and VII, the text, and the Appendix. Data points are ratios of the observed cross sections to predicted $\langle\sigma_r\rangle$. Points omitted from the search are indicated by arrows or open circles.

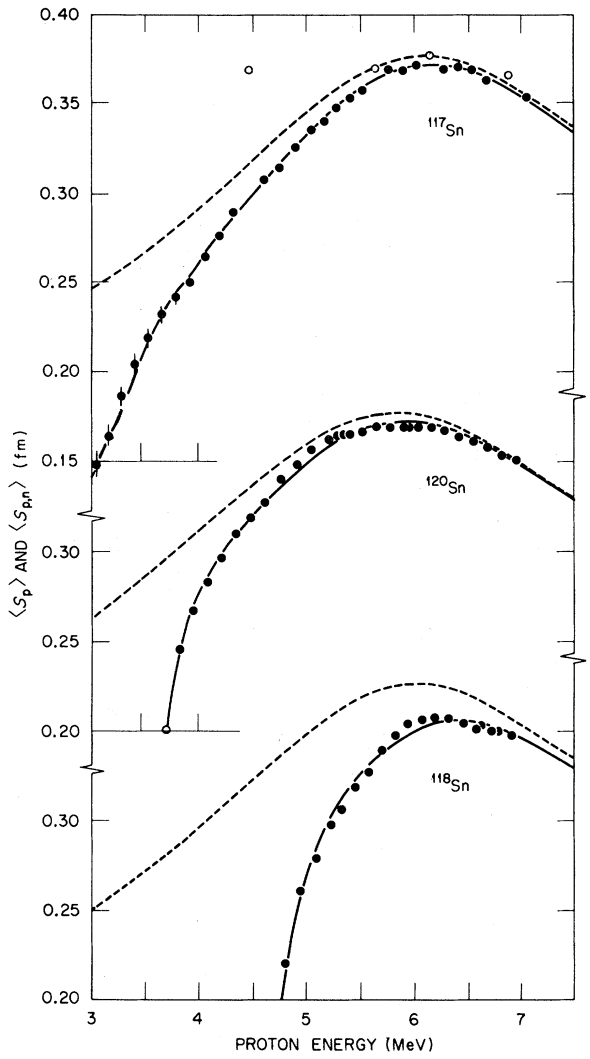

FIG. 15. Global analysis of ^{117,118,120}Sn. Data points are observed $\langle S_{p,n}\rangle$; open circles were omitted from the search. Solid curves are fitted $\langle S_{p,n}\rangle$, see Fig. 14 caption. Dashed curves are predicted $\langle S_p\rangle$ for parameters of Tables IV and VII.

and the observed cross sections divided by the same $\langle\sigma_r\rangle$. We emphasize that these data points, unlike the strength functions, are interpretations based on theoretical $\langle\sigma_r\rangle$. The fluctuations are significant. Broad maxima are observed at about 1.5 MeV above threshold for ^{118}Sn and ^{120}Sn and are mostly responsible for the large χ^2 for these two targets. Figure 15 shows the fits to the experimental $\langle S_{p,n}\rangle$ for ^{117,118,120}Sn and the predicted $\langle S_p\rangle$ (dashed curves). The fitted curves of $\langle S_{p,n}\rangle$ for ^{119,122,124}Sn are not shown but are nearly the same as the three-parameter fits of $\langle S_p\rangle$ in Figs. 10 and 11 (except at high energies for ^{119}Sn). The dashed curve in Fig. 11 is the global $\langle S_p\rangle$ for ^{119}Sn. Figure 12(b) shows $\langle S_p\rangle$ for all six targets.

TABLE VIII. Refitted parameters (fixed parameters listed in Table IV) to published ^{120}Sn+p differential scattering cross sections.

E_p (MeV)	χ^2	$V_R(E_p)$ (MeV)	W_D (MeV)	a_D (MeV)	J_R/A (MeV fm^3)	J_D/A (MeV fm^3)
9.8[a]	0.72	58.13	16.13	0.400	484	112.6
16[b]	17.1	54.36	10.67	0.631	453	119.7

[a] Reference 22.
[b] Reference 26.

VIII. DISCUSSION

The following includes comparisons with elastic scattering at higher proton energies. To reduce the ambiguities in parametrization we have reanalyzed some proton differential cross sections using the same fixed and adjustable parameters as above. Table VIII lists $V_R(E)$, W_D, and a_D to fit the precision ^{120}Sn(p,p) differential cross sections reported at 9.8 MeV [22] and 16 MeV.[26]

In the present work three optical-model quantities and their isotopic dependences have been deduced from the observed heights, widths, and spacings of the p-wave strength-function resonances in Sn. Of these three, one is related to the real potential and two to the absorptive potential.

A. Real potential

In Table VII the essential quantity for the real well for each isotope is VR^2 at the resonant peak and it is invariant to ±1% in respect to all other parameters of the model. Comparisons with the elastic scattering parameters for ^{120}Sn in Table VIII show that $V_R(0)$ and J_R/A are larger here than at 10 and 16 MeV. Continuity requires $b_0 = 0.88$ MeV^{-1} from 5.75 to 10 MeV and 0.61 MeV^{-1} from 10 to 16 MeV. As discussed below, the disagreement with the b_0 of 0.32 MeV^{-1} used here suggests that the potential is l dependent.

The isotopic dependence for the real potential comes out simply; the volume integral per nucleon J_R/A at the resonant energy for each isotope is constant, 513.5 MeV fm^3. This constant is essentially invariant with respect to all of the model parameters except r_R, and it varies linearly with r_R. The value of 513.5 MeV fm^3 is for a radius of $1.2A^{1/3}$. If some dependence other than $A^{1/3}$ were assumed, J_R/A would vary accordingly.

The values of J_R/A were not expected to be constant. Larger increases were expected in VR^2 from ^{117}Sn to ^{124}Sn with corresponding larger spacings in resonant energies. That is illustrated by the predicted resonances in Fig. 5. There are three reasons for this: (1) The radii increase with mass number; an $A^{1/3}$ dependence is assumed. (2) The strength of the potential was expected to increase as $V_{R1}\epsilon$, where V_{R1} is the asymmetry potential of about 25 MeV.[42] (3) Since these first two effects shift the resonant energy, the energy dependence in the real local potential shifts it further; the b_0E term for the predictions was assumed to be large enough to make the potential for the $3p$ resonance continuous with that for all partial waves at 10 MeV, i.e., $b_0 \simeq 0.88$ MeV^{-1}. (The Coulomb correction works in the opposite direction to these three but its effect is negligible, particularly since the charge radii vary only as $A^{1/6}$.)

One or more of these three effects had to be reduced from the predictions in order to describe the smaller spacings observed. In regard to the radii, the observed[25] matter radii for the even Sn isotopes actually require a stronger dependence, $A^{0.6}$, for an assumed constant diffuseness a_R. We retained the smaller $A^{1/3}$ dependence because the predicted spacings were already too large. (Then the matter radii require that a_R increase with A such that J_R/A increases by 0.9% from ^{117}Sn to ^{124}Sn.)

Having assumed the $A^{1/3}$ dependence we had to reduce either the E or ϵ dependence, or both. Figure 7(b) showed that either or both could be reduced. One possibility would have been to keep either b_0 or V_{R1} fixed at the expected value; however, that would have required the other one to go negative. Our decision was to reduce both.

We abandoned the requirements of continuity with the potential at higher energies. This is equivalent to assuming an l dependence in the potential. The b_0 used here, 0.32 MeV^{-1}, came from a global analysis[18] of many nuclei at higher energies and is reasonable for a local potential. It gave the best fit [Fig. 7(b)] for the ^{124}Sn(p,n) cross sections, there is some justification[43] for a small energy dependence at low energies for near-spherical nuclei such as Sn, and a further justification is given below in relation to the asymmetry potential.

Since the resulting ϵ dependence is almost zero we have used [Eq. (24)] the notation $V_\epsilon\epsilon$ rather than $V_{R1}\epsilon$ to emphasize that the observed isotopic dependence seems unrelated to the usual neutron-

proton asymmetry potential, which surely exists and is discussed below. It appears that, as neutrons are added to in the Sn isotopes, the condition for the $3p$ resonance is simply that the volume integral per nucleon of the real potential remains constant.

There are similar observations on the asymmetry potential in the literature. The volume integral per nucleon at a given proton energy is expected to increase with ϵ; nevertheless, Boyd *et al.*[25] found, with large uncertainties, no increase for the Sn isotopes. Greenlees *et al.*[24] found a general lack of ϵ dependence in the proton potential for other nuclei, but those conclusions have been contested by Sood and Agrawal.[44]

B. Absorptive potential

In Table VII the values for the absorptive volume integral per nucleon, J_D/A, are nearly constant, 80.5 ± 0.5 MeV fm^3, and about 30% smaller than deduced in Table VIII from elastic scattering at 10 and 16 MeV. Uncertainties propagated from ambiguities in other parameters are about ±4%; therefore, $J_D/A = 80 \pm 4$ MeV fm^3. This is smaller than the 115 ± 15 MeV fm^3 deduced by Agrawal and Sood[17] for the total volume-plus-surface absorption by 10- to 60-MeV protons on many different nuclei, and it indicates that J_D/A decreases rather abruptly below 10 MeV. General theoretical treatments[45] suggest that the Pauli exclusion principle and nuclear correlations at lower energies tend to decrease the absorptive potential, but this is apparently not so from 10 to 60 MeV. Another possible explanation is that the potential is l dependent such that the value for p waves is smaller than the average determined for all partial waves at higher energies.

The other parameter is the diffuseness a_D. It is found to increase 10% from ^{117}Sn to ^{124}Sn. The study of parameter space (Figs. 6–8) shows that it is determined to ±10% without the usual "$W_D a_D$ ambiguity" and without other ambiguities except for the geometry of the real well. With the ambiguities of the real well included, $a_D = 0.4 \pm 0.1$ fm.

C. Asymmetry potentials

Comparisons can be made between the positions and widths of these $3p$ proton resonances and the well-known $3p$ neutron resonance. Since the $3p$ proton state in Sn is quasibound by an 8-MeV Coulomb barrier, it is observable as in the present work even though its spreading width is several MeV. The neutron state is not quasibound by a barrier comparable to this width but it is still observed at low neutron energies as a size resonance, i.e., as a function of the atomic weight.

Recently Camarda[46] deduced p-wave strength functions near $A = 100$ from precision transmission measurements for neutron energies near 100 keV. Figure 16 shows Camarda's points including those quoted[47,48] from earlier precision measurements.

The dashed curve in Fig. 16 is calculated for nuclei along the valley of β stability ($A/Z = 2 + 0.015A^{2/3}$) using a model with parameters that are the same except for the real-well depth as those deduced here for ^{118}Sn, which is also in the valley of stability. If only the Coulomb potential were omitted the peak would be at somewhat lower A. The position of the peak has been brought up to give a peak at $A = 94$ by reducing the real-well depth to 52 MeV, which is 9.6 MeV less than that at the 6-MeV proton resonance in ^{118}Sn.

This reduction in the well depth is essentially a reduction in VR^2. A change in the real potential is expected for three reasons[42] in addition to the $A^{1/3}$ radial dependence: (1) An asymmetry term arises from the isospin potential. (2) The energy dependence $b_0 E$ results in a deeper well for 0.1-MeV neutrons than for 6-MeV protons. (3) If the energy dependence is due to the actual nonlocality of the potential, there should be a correction for protons due to the energy dependence of the interaction and the Coulomb potential felt by the protons. In summary, and in lowest order,[42]

$$V_{Rp}(E_p) = V_{R0} + \epsilon_p V_{R1} - b_0 E_p + \tfrac{6}{5} b_0 (Ze^2/R_C)_p$$

and (25)

$$V_{Rn}(E_n) = V_{R0} - \epsilon_n V_{R1} - b_0 E_n ,$$

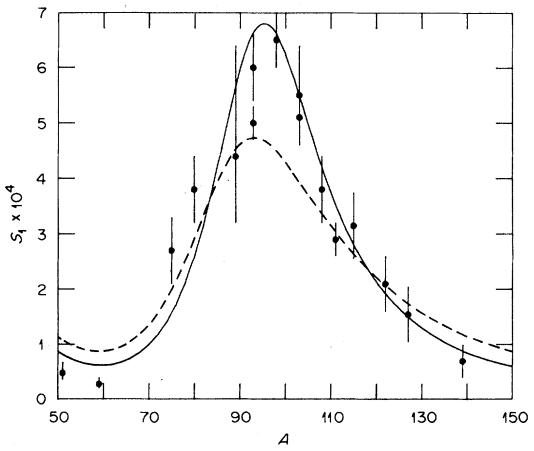

FIG. 16. Predicted and observed p-wave strength functions for 0.1-MeV neutrons. Points are from Camarda (Ref. 46) and other references (Refs. 47 and 48) cited therein. The dashed curve is calculated with global parameters (Tables IV and VII) except $V_R(E_n) = 52$ MeV. The solid curve includes a 15-MeV asymmetry term in the absorptive potential such that, for example, $W_D = 7.4$ MeV at $A = 94$. Both theory and experiment have been reduced to the same units (Ref. 46) using $r_0 = 1.4$ fm.

where the subscripts n and p refer to neutrons and protons incident on different nuclei.

Substituting $1.22A^{1/3}$ for R_C and solving, we find

$$V_{R1} = \frac{V_{Rp}(E_p) - V_{Rn}(E_n) - b_0[1.42(Z/A^{1/3})_p - (E_p - E_n)]}{\epsilon_p + \epsilon_n}, \quad (26)$$

so the asymmetry potential V_{R1} required for a 6-MeV resonance for protons on ^{118}Sn and a size resonance at $A = 94 \pm 3$ for 0.1-MeV neutrons is 24 ± 3 MeV, in good agreement with the accepted value[42] of about 25 MeV.

This ± 3-MeV uncertainty is only that propagated from $\Delta A = \pm 3$. The result is sensitive to b_0. As stated above, we could have increased b_0 without changing VR^2. If, for example, we had increased b_0 to be consistent with the 10-MeV proton scattering, then $V_{R1} = 7$ MeV. The Coulomb correction also has uncertainties, so these results, like many others, are not definitive on the asymmetry potential. However, if the 25-MeV asymmetry potential is assumed, these results support the small b_0 in the real potential and the corresponding l dependence discussed above.

An asymmetry term is expected also in the absorptive potential; however, the above dashed curve (Fig. 16) was calculated with zero asymmetry, i.e., the same absorptive potential ($W_D = 11.7$ MeV) for neutrons along the valley of stability as for protons incident on ^{118}Sn. The curve disagrees with the height of the experimental peak. Satchler[42] found the asymmetry potential to be about 15 MeV, and the solid curve in Fig. 16 was calculated with that value. Then $W_D = 7.4$ MeV at $A = 94$. The resulting agreement with the experimental strengths supports an absorptive asymmetry of about 15 MeV.

D. Partial failure of the statistical model

The above statistical model predictions of the ratio of (p,n) to total reaction cross sections were mostly successful but suggest serious discrepancies in compound nuclear temperatures or some other aspect of the model. The model uses available data on particle transmission factors, low-lying states, level densities, and radiative widths. In Table VII the required γ-ray normalizations, $T_{\gamma 0}(E_0)/T_1 = 2 \pm 1$, are reasonable in light of the uncertainties in level densities and radiative widths that enter into the transmission factors, $2\pi\rho\Gamma_\gamma$.

However, the required energy derivatives D_x are outside of expected limits. If one assumes, as we have in Eq. (22), that D_x is a property of the compound excited states, then it is approximately $2\sqrt{a}$ and has an expected uncertainty of only $\pm 10\%$ because the experimental density parameters in this mass region[37] are in the range $13 < a < 16$ MeV^{-1}. The normalizations of 0.39 and 0.63 in Table VII indicate that the compound nuclear temperatures are about a factor of 2 higher than expected. The same conclusion would result if the strength function $f(E_\gamma)$ were altered to include the pigmy resonance[39] because the functional form of $f(E_\gamma)$ determines mostly the normalization rather than the energy dependence of $T_{\gamma 0}(E_x)$. (An alternate but essentially equivalent interpretation can be made. The energy derivative D_x could be written with reference to Γ_γ/Γ_n, so that it would be a combined property of the compound and residual nuclei. Then, at higher proton energies where most neutrons go to the residual continuum, it would be approximately proportional to the difference in reciprocal temperatures for the compound and final nuclei. The uncertainties in this difference are smaller than in the compound temperature by itself; nevertheless, the normalizations are outside the limits. This ambiguity in the meaning of D_x disappears at lower proton energies where neutrons go only to the known low-lying states. For protons below about 5 MeV on ^{117}Sn, in particular, D_x refers to the compound system.)

A different explanation of the discrepancy would be that the neutron widths are not properly described by the statistical model using optical-model transmission factors. A third explanation would be that Γ_n/Γ_γ really does increase slowly with energy and that the proton strength functions just happen to have the isotopic sequence in Fig. 12(a) to cancel this increase. By assumption in this paper we have discarded this latter explanation.

E. Probable broad structures in ^{118,120}Sb

The broad maxima in Fig. 14 at about 1.5 MeV above threshold for ^{118,120}Sn are statistically significant and probably due to structures in the residual nuclei rather in the highly excited compound states. Although these fluctuations are small, they require large variations in Γ_γ/Γ_n and indicate a grouping of levels of high density or low spins at about 1 to 1.5 MeV excitation in the odd-odd nuclei.

IX. CONCLUSIONS

Proton strength function resonances due to the $3p$ quasibound state have been clearly observed. This is apparently the first observation of size resonances for incident nucleons as a function of incident energy. The position, height, and width of the resonance in each Sn isotope are well described by adjusting three parameters in the opti-

cal-model potential. The resonant energies are unambiguously related to VR^2 for the real potential at the resonance. The volume integrals per nucleon for both the absorptive and real potentials are determined with little ambiguity for p waves. The diffuseness of the absorptive potential is determined without ambiguity to ±30%.

Several questions remain. Does the small volume integral for the absorptive potential and the large integral for the real potential really indicate an l dependence for both? Is the observed isotopic dependence on the real-well volume integral per nucleon a fundamental requirement for resonance? Does the exact isotopic sequence also imply an exact isotonic sequence or is it a special feature of spherical nuclei such as Sn? Does the asymmetry potential have anything to do with these sequences? Is a different interpretation[49] more appropriate? It appears that interesting results would come from further study of these resonances for other nuclei in this mass region.

ACKNOWLEDGMENTS

We are grateful to Dr. G. R. Satchler and Dr. J. A. Holmes for helpful discussions of the optical and statistical models. We are indebted to Dr. V. Spiegel for the loan of the National Bureau of Standards neutron source.

APPENDIX

A. Levels in ^{117,119}Sb

The odd Sb isotopes have similar simple structures associated with the 51st proton and have been studied extensively. Vanden Berghe and Heyde[50] made predictions from the particle-core coupling model using five proton orbits ($3s_{1/2}$, $2d_{3/2}$, $2d_{5/2}$, $1g_{7/2}$, $1h_{11/2}$) and all combinations of quadrupole and octupole phonon states up to an unperturbed energy of 5.5 MeV. Vanden Berghe and Degrieck[51] included two-particle–one-hole states. Their predictions are excellent guides for resolving uncertain experimental assignments.

Table IX lists levels with $J \leq \frac{11}{2}$ observed below 2 MeV. These are from the ^{118}Sn(^{3}He, d) reaction,[52,53] the ^{116}Cd(^{6}Li, $3n$) reaction,[54] the ^{119}Sn(p, n) reaction[5,55] and from measurements[53,55-58] of the γ rays following β decay of $\frac{11}{2}^-$ and $\frac{1}{2}^+$ states in ^{119}Te. The (p, n) reaction was studied by measuring neutron energies[5] and γ rays[55] from (p, $n\gamma$). Since this reaction is nonselective, except for centrifugal barrier effects, it missed only the three high-spin states with $J^\pi = \frac{9}{2}^-$, $\frac{11}{2}^-$, and $\frac{11}{2}^+$ that would require f-wave particles. The J^π assignments below 1.5 MeV are either certain or highly probable. Above 1.5 MeV the $\frac{3}{2}^+$ and one of the $\frac{1}{2}^+$ assignments are definite[5] and experimental limits are known for the other levels. We made the other assignments partly on the basis of theory.[50] Errors in assignments would have minor effects on the statistical calculations. Errors due to missed levels would be more important; however, significant levels are not expected to be missed because the (p, n) reaction that is to be calculated was used to detect these levels.

The levels of ^{117}Sb are known less reliably but, since these nuclei are similar, the data on ^{119}Sn can supplement ^{117}Sb. Table IX includes levels of ^{117}Sb from the above references on ^{119}Sb, and some assumed levels (in parentheses) based on comparisons with ^{119}Sb. Those observed are from

TABLE IX. Known and assumed levels in ^{117,119}Sb. For ^{119}Sb all energies are experimental and the J^π values are known or are probable assignments from theory and experiment. The assumed levels for ^{117}Sb are shown in parentheses.

J^π	Excitation energies (keV) ^{119}Sb	^{117}Sb
$\frac{5}{2}^+$	0	0
$\frac{7}{2}^+$	270	525
$\frac{1}{2}^+$	644	720
$\frac{3}{2}^+$	700	924
$\frac{9}{2}^+$	970	1160
$\frac{7}{2}^+$	1048	1085
$\frac{9}{2}^+$	1213	1300
$\frac{9}{2}^+$	1250	(1310)
$\frac{1}{2}^-$	1327	1355
$\frac{3}{2}^+$	1339	1380
$\frac{11}{2}^-$	1366	1320
$\frac{11}{2}^+$	1341	1534
$\frac{9}{2}^-$	1407	(1410)
$\frac{3}{2}^-$	1413	1420
$\frac{1}{2}^-$	1488	1455
$\frac{7}{2}^+$	1547	(1600)
$\frac{5}{2}^+$	1647	(1640)
$\frac{1}{2}^+$	1660	(1660)
$\frac{3}{2}^+$	1750	1716
$\frac{1}{2}^+$	1821	1810
$\frac{5}{2}^+$	1848	1880
$\frac{3}{2}^+$	1875	(1900)
$\frac{7}{2}^+$	1982	2010

TABLE X. Fictive ground states for Sb isotopes.

A	Δ (MeV)	Levels	Interval (MeV)
117	0.7	20	0.9 to 2.05
118	−0.5	50	0.0 to 1.22
119	0.7	19	0.9 to 2.0
120	−0.5		
121	0.7		
122	−0.9	17	0.0 to 0.5
123	0.7		

^{116}Sn(^{3}He,d), ^{114}Cd(^{6}Li,$3n\gamma$), ^{117}Sn(p,n), and from the γ rays following the β decay of ^{117}Te($\frac{1}{2}^{+}$). All observed levels show good correspondence with ^{119}Sb in energy and known or probable J^{π}. Levels from the nonselective (p,n) extend up to 1.5 MeV; in that region the low-spin levels correspond one-to-one to those in ^{119}Sb. Some levels found above 1.5 MeV by (p,n) in ^{119}Sb were missed in ^{117}Sb by the more selective reactions. There is little uncertainty in the J^{π} assignments below 1.5 MeV; above 1.5 MeV the assignments rely heavily on ^{119}Sb.

B. Levels in ^{118,120,122}Sb

The level structures in the residual odd-odd nuclei are less certain and more complicated. Some ideas can be deduced from simple shell-model arguments.[59] In the odd-even nuclei the $2d_{5/2}$ and $1g_{7/2}$ proton orbits compete for the ground state, and the $3s_{1/2}$ and $1g_{7/2}$ states are near 0.7 MeV. In the even-odd Sn nuclei the $3s_{1/2}$, $3d_{3/2}$, and $1h_{11/2}$ neutron orbits compete for the ground state and the $1g_{7/2}$ particle-hole state is near 0.7 MeV. The odd-odd hierarchy of states produced by simple coupling of these orbits include 24 levels with $J \leq 2$ and $J^{\pi} = 3^{+}$ which could be populated by the ^{118,120}Sn(p,n) reactions with various combinations of s- and p-wave proton and neutrons. The hierarchy also has 14 states with $J^{\pi} = 3^{-}$, 4^{-}, 4^{+}, and 5^{+} which could be populated by d waves for either or both particles.

Chaffee *et al.*[60,29] studied ^{118}Sb by various reactions, particularly by ^{118}Sn($p,n\gamma$). They attributed 118 γ-ray lines to states below 1200 keV in ^{118}Sb and, using coincidence measurements on the more intense lines, established 24 levels including the 1^{+} ground state. The weaker γ rays gave evidence for 14 additional levels below 1200 keV. We have assumed that the first 24 levels are populated by combinations of s- and p-wave particles and, therefore, assign J^{π} essentially from the above hierarchy of 24 lower spin levels, with the requirement that nearly all of the observed transitions can be dipole. In like manner we assign J^{π} values to the weaker 14 levels from the higher 14 levels of the hierarchy. Little is known[33] about the levels in ^{120}Sb. Since ^{118}Sb and ^{120}Sb are expected to have similar structures, we assume the same for both. The low-lying levels in ^{122}Sb are not critical because γ-ray competition in the ^{122}Sn(p,n)^{122}Sb reaction is almost negligible for proton energies above 3 MeV. We use the 18 levels listed below 500 keV by Bertrand[61] and make J^{π} assignments similar to ^{118}Sb above.

C. Fictive ground states

Given $a = 15$ MeV^{-1} we normalized the density formula to the low-lying levels of each nucleus by adjusting Δ to make the total predicted levels, $\int \rho(U)\,dU$, for a given energy interval the same as the number observed or expected from the systematics of neighboring nuclei. [The lower limit of the integral must be above the minimum in $\rho(U)$.] Table X lists for each Sb isotope the energy interval, the number of observed levels, and Δ. For ^{117}Sb and ^{119}Sb the number of levels are from Table IX. For ^{121}Sb and ^{123}Sb fewer levels have been reported[62-65] than for ^{119}Sb; nevertheless, we assume the same Δ because the number of states is not expected[50] to decrease with increasing neutron number. For ^{118}Sb a value of −0.4 MeV would be required to account for the 38 states discussed above but we have assigned $\Delta = -0.5$ MeV, corresponding to 50 states, because there is evidence[66] for more levels in this region. Also, for ^{120}Sb we assume $\Delta = -0.5$ MeV. Levels in ^{122}Sb are from Bertrand.[61] The ^{124,125}Sb nuclei are not included in the table because the corrections for ^{124}Sn(p,n)^{124}Sb are negligible. In similar manner we assigned Δ for each Sn target.

---

*Student (1970) from Virginia Polytechnic Institute, Blacksburg, Virginia.

†Research sponsored by the U. S. Energy Research and Development Administration under contract with Union Carbide Corporation.

[1]C. H. Johnson and R. L. Kernell, Phys. Rev. Lett. 23, 20 (1969); Phys. Rev. C 2, 639 (1970).

[2]H. H. Barschall, Phys. Rev. 86, 431 (1952).

[3]J. D. Lawson, Phil. Mag. 44, 102 (1953); H. H. Barschall (private communication).

[4]H. J. Kim, R. L. Robinson, R. L. Kernell, and C. H. Johnson, Phys. Rev. Lett. 19, 325 (1967).

[5]R. L. Kernell, H. J. Kim, R. L. Robinson, and C. H. Johnson, Nucl. Phys. A176, 449 (1971).

[6]P. Richard, C. F. Moore, J. A. Becker, and J. D. Fox, Phys. Rev. 145, 971 (1966).
[7]J. L. Fowler, C. H. Johnson, and R. M. Feezel, Phys. Rev. C 8, 545 (1973).
[8]J. B. Marion, Rev. Mod. Phys. 38, 660 (1966).
[9]R. L. Macklin, Nucl. Instrum. 1, 335 (1957).
[10]A. DeVolpi and K. G. Porges, Phys. Rev. C 1, 683 (1970).
[11]M. E. Anderson, Nucl. Appl. Technol. 4, 142 (1968).
[12]R. L. Bramblett and T. W. Bonner, Nucl. Phys. 20, 395 (1960).
[13]R. M. Wood, R. R. Borchers, and H. H. Barschall, Nucl. Phys. 71, 529 (1965).
[14]C. H. Johnson, A. Galonsky, and J. P. Ulrich, Phys. Rev. 109, 1243 (1958).
[15]C. H. Johnson, C. C. Trail, and A. Galonsky, Phys. Rev. 136, B1719 (1964).
[16]R. Collé, R. Kishore, and J. B. Cumming, Phys. Rev. C 9, 1819 (1974).
[17]D. C. Agrawal and P. C. Sood, Phys. Rev. C 11, 1854 (1975).
[18]F. D. Becchetti, Jr., and G. W. Greenlees, Phys. Rev. 182, 1190 (1969).
[19]J. R. Ficenec, L. A. Fajardo, W. P. Trower, and I. Sick, Phys. Lett. 42B, 213 (1972).
[20]F. G. Perey (private communication).
[21]M. Reeves, III (private communication).
[22]G. W. Greenlees, C. H. Poppe, J. A. Sievers, and D. L. Watson, Phys. Rev. C 3, 1231 (1971).
[23]G. W. Greenlees, G. J. Pyle, and Y. C. Tang, Phys. Rev. 171, 1115 (1968)
[24]G. W. Greenlees, W. Makofske, and G. J. Pyle, Phys. Rev. C 1, 1145 (1970).
[25]R. N. Boyd, J. Fenton, M. Williams, T. Kruse, and W. Savin, Nucl. Phys. A162, 497 (1971).
[26]W. Makofske, G. W. Greenlees, H. S. Liers, and G. J. Pyle, Phys. Rev. C 5, 780 (1972).
[27]E. Vogt, in *Advances in Nuclear Physics*, edited by M. Baranger and E. Vogt (Plenum, New York, 1968), Vol. I, p. 261.
[28]P. A. Moldauer, Phys. Rev. 135, B642 (1964).
[29]G. H. Carlson, W. L. Talbert, Jr., and S. Raman, Nucl. Data Sheets 17, 1 (1976).
[30]P. A. Baedecker, A. Pakkanen, and W. B. Walters, Nucl. Phys. A158, 607 (1970).
[31]P. H. Stelson, W. T. Milner, F. K. McGowan, R. L. Robinson, and S. Raman, Nucl. Phys. A190, 197 (1972).
[32]S. Raman, P. H. Stelson, G. G. Slaughter, J. A. Harvey, T. A. Walkiewicz, G. J. Lutz, L. G. Multhauf, and K. G. Tirsell, Nucl. Phys. A206, 343 (1973).
[33]D. C. Kocher, Nucl. Data Sheets 17, 39 (1976).
[34]D. Wilmore and P. E. Hodgson, Nucl. Phys. 55, 673 (1964).
[35]J. R. Huizenga, L. G. Moretto, Annu. Rev. Nucl. Sci. 22, 427 (1972).
[36]A. Gilbert and A. G. W. Cameron, Can. J. Phys. 43, 1446 (1965).
[37]W. Dilg, W. Schantl, H. Vonach, and M. Uhl, Nucl. Phys. A217, 269 (1973).
[38]*Resonance Parameters*, compiled by S. F. Mughabghab and D. I. Garber, Brookhaven National Laboratory Report No. 325, 3rd ed., Vol. 1 (National Technical Information Service, Springfield, Virginia, 1973).
[39]G. A. Bartholomew, E. D. Earle, A. J. Ferguson, J. W. Knowles, and M. A. Lone, in *Advances in Nuclear Physics*, edited by M. Baranger and E. Vogt (Plenum, New York-London, 1973), Vol. 7, p. 229.
[40]D. M. Brink, Ph.D thesis, Oxford University, Oxford, England, 1955 (unpublished).
[41]P. Axel, Phys. Rev. 126, 671 (1962).
[42]G. R. Satchler, in *Isospin in Nuclear Physics*, edited by D. H. Wilkinson (North-Holland, Amsterdam, 1969), Chap. 9.
[43]F. G. Perey, Phys. Rev. 131, 745 (1963).
[44]P. C. Sood and D. C. Agrawal, Indian J. Pure Appl. Phys. 11, 571 (1973).
[45]P. E. Hodgson, *The Optical Model of Elastic Scattering* (Clarendon, Oxford, England, 1963), p. 171.
[46]H. S. Camarda, Phys. Rev. C 9, 28 (1974).
[47]C. A. Uttley, C. M. Newstead, and K. M. Diment, in *Proceedings of the Conference on Nuclear Data, Microscopic Cross Sections and Other Data Basic for Reactors, Paris, 1966* (International Atomic Energy Agency, Vienna, 1967), Vol. 1, p. 165.
[48]J. Morgenstern, R. N. Alves, J. Julien, and C. Samour, Nucl. Phys. A123, 561 (1969).
[49]V. K. Sirotkin and V. D. Chesnokova, Izv. Akad. Nauk SSSR Ser. Fiz. 35, 2359 (1971) [Bull. Acad. Sci. USSR Phys. Ser. 35, 2140 (1972)].
[50]G. Vanden Berghe and K. Heyde, Nucl. Phys. A163, 478 (1971).
[51]G. Vanden Berghe and E. Degrieck, Z. Phys. 262, 25 (1973).
[52]T. Ishimatsu, K. Yagi, H. Ohmura, Y. Nakajima, T. Nakagawa, and H. Orihara, Nucl. Phys. A104, 481 (1967).
[53]J. Kantelle, J. Hattula, T. Hattula, H. Kalm, and O. J. Marttila, Ann. Acad. Sci. Fenn. A VI, 259 (1967).
[54]A. K. Gaigalas, R. E. Shroy, G. Schatz, and D. B. Fossan, Phys. Rev. Lett. 35, 555 (1975).
[55]R. Duffait, A. Charvet, and R. Chéry, Z. Phys. A272, 315, 321 (1975).
[56]G. Berzins and W. H. Kelly, Nucl. Phys. A92, 65 (1967).
[57]G. Graeffe, E. J. Hoffman, and D. G. Sarantites, Phys. Rev. 158, 1183 (1967).
[58]V. A. Shilin and V. R. Burmistrov, Izv. Akad. Nauk SSSR Ser. Fiz. 36, 2509 (1972) [Bull. Acad. Sci. USSR Phys. Ser. 36, 2181 (1972)].
[59]S. A. Hjorth, Ark. Fys. 33, 183 (1967).
[60]W. B. Chaffee, C. B. Morgan, J. A. Guile, R. A. Warner, L. E. Samuelson, W. H. Kelly, W. C. McHarris, E. M. Bernstein, and R. Shamu, Michigan State University Cyclotron report, 1972–1973 (unpublished).
[61]F. E. Bertrand, Nucl. Data B7, 419 (1972).
[62]D. J. Horen, Nucl. Data B6, 75 (1971).
[63]R. L. Auble, Nucl. Data B7, 363 (1972).
[64]E. C. Booth, R. G. Arnold, and W. G. Alston, III, Phys. Rev. C 7, 1500 (1973).
[65]M. Conjeaud, S. Harar, M. Caballero, and N. Cindro, Nucl. Phys. A215, 383 (1973).
[66]W. H. Kelly (private communication).